

**NOT FOR
PUBLIC RELEASE**

Metamorphic Evolution of the Ribeira Belt: Evidence from Outcrops in the Rio de Janeiro Area, Brazil

A. KÜHN^{1*}, K. STÜWE¹ AND R. A. J. TROUW²¹DEPARTMENT OF GEOLOGY AND PALAEOLOGY, UNIVERSITY OF GRAZ, HEINRICHSTRASSE 26, 8010 GRAZ, AUSTRIA²UNIVERSIDADE FEDERAL DO RIO DE JANEIRO, DEPARTAMENTO DE GEOLOGIA, CEP 21910-900 RIO DE JANEIRO, BRAZIL

RECEIVED JULY 26, 2003; ACCEPTED JULY 5, 2004

Migmatitic granulites and arc-related felsic intrusives of Pan-African age form the bedrock in the Rio de Janeiro area, SE Brazil. These rocks preserve a partial record of three parageneses. The earliest assemblage (M₁) grew during fabric formation in the rocks (D₁) and is characterized by the mineral assemblage Pl + Bt + Sil + Kfs + Qtz. Peak metamorphic conditions (M₂) are characterized by the assemblage Bt + Crd + Kfs + Pl + Grt + liq + Qtz and are inferred to have developed during D₂ folding of the rocks at T = 750–800°C and P = 7 kbar. M₃ reaction textures overprint the M₂ assemblage and comprise symplectitic intergrowth of cordierite(II) and quartz that formed after garnet, whereas secondary biotite formed as a result of reactions between garnet and K-feldspar. By comparing the observed modal abundances with modal contours of garnet, cordierite and quartz on the relevant pseudosection a post M₂ P–T vector indicating contemporaneous cooling and decompression can be deduced. The inferred equilibrium assemblage and reaction textures are interpreted to reflect a clockwise P–T path involving heating followed by post-peak decompression and associated cooling. We infer that metamorphism occurred in response to advective heating by the abundant syn-collisional (arc-related) I-type granitoids in the region, consistent with the unusually high peak T/P ratio.

KEY WORDS: *advective heating; Ribeira belt; granulite; partial melting; P–T pseudosection*

INTRODUCTION

Low-pressure granulite-facies terrains are generally defined as those with peak metamorphic assemblages in

metapelites involving garnet–cordierite equilibria (i.e. around 750°C and above) and formation pressures below and sometimes dramatically below 7 kbar (e.g. see Greenfield *et al.*, 1998), corresponding to a crustal depth of less than about 25–30 km. Two major groups of models have been invoked to explain the unusually high temperature/pressure ratios reported from these rocks. Some workers have argued that the high temperatures can be attained only if advective heat sources contributed to the heating of these terrains; i.e. they are contact metamorphic terrains in the widest sense (Lux *et al.*, 1986; Hanson & Barton, 1989; Guidotti, 2000). Others have argued that advective heat sources (e.g. abundant granitoids) are rarely observed in the immediate vicinity of these terrains and that they can be explained in terms of conductive geotherms in unusual tectonic settings (e.g. Harley, 1989; Sandiford & Hand, 1998; Solar & Brown, 2000).

To address the heat source controversy, metamorphic petrologists have derived *P–T* paths for many low-*P*/high-*T* terrains. Interestingly, a large variety of *P–T* paths has been discovered in otherwise very similar terrains [see summary by Harley (1989)]. *P–T* evolutions involving isothermal decompression (e.g. Stüwe & Powell, 1989*a*; Brown & Raith, 1996; Carson *et al.*, 1997) have often been used to argue for a Barrovian-type metamorphic evolution, whereas *P–T* paths characterized by isobaric cooling (Vernon, 1982) or compression with cooling (Stüwe & Powell, 1989*b*) have been used to argue for advective heating mechanisms.

*Corresponding author. Present address: Institute for Geosciences, University of Mainz, Becherweg 21, D-55099 Mainz, Germany. Telephone: 0049 (0)6131 3924368. Fax: 0049 (0)6131 3924769. E-mail: kuehna@uni-mainz.de

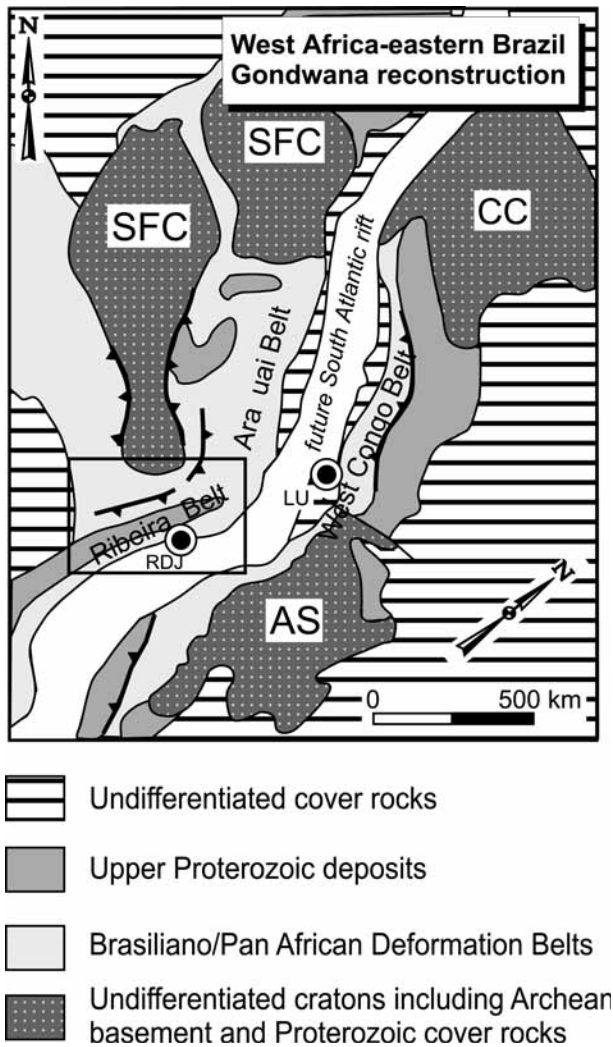


Fig. 1. Jurassic Gondwana reconstruction prior to the opening of the South Atlantic, showing the location of the major cratonic areas and Brasiliano–Pan-African mobile belts (after Cunningham *et al.*, 1998; Brueckner *et al.*, 2000). RDJ, Rio de Janeiro; LU, Luanda; SFC, São Francisco Craton; CC, Congo Craton; AS, Angola Shield.

One area comprising regional metamorphism of apparently low- P /high- T granulite facies in the immediate vicinity of granitoid intrusions of the same age is the Ribeira belt around Rio de Janeiro in Brazil (Figs 1 and 2). There, syn-collisional to late collisional Pan-African–Brasiliano granitoids intrude a metapelitic sequence that suffered peak metamorphism at the same time (Heilbron, 1995; Machado *et al.*, 1996; Machado, 1997; Brueckner *et al.*, 2000; Valladares *et al.*, 2000). Outcrop-scale reaction textures of cordierite after garnet along Copacabana and Ipanema beaches (Fig. 2) apparently indicate post-peak decompression. However, these rocks are located in the immediate vicinity of abundant syn-tectonic intrusions, apparently providing an ideal ‘advective heat

source’. As such, the terrain may be an example where a clockwise P – T path is demonstrably related to an advectively heated terrain and cannot be used as an argument for Barrovian-type metamorphic cycles.

To test this idea we present a careful analysis of the petrography, mineral chemistry and reaction textures from Al-rich granulite-facies metapelites of the Ribeira belt in the Rio de Janeiro area and infer a probable P – T path for these rocks. On the original maps (Helmbold *et al.*, 1964) these rocks comprise garnet-, sillimanite- and cordierite-bearing mineral assemblages, which were referred to as kinzigites [following the original definition of kinzigites from Fischer (1861)], and we follow this terminology here. The P – T path is discussed within the tectonic framework of the region and in terms of possible heat sources of metamorphism.

REGIONAL GEOLOGICAL SETTING

Southeast Brazil is made up of cratonic areas (Early Proterozoic to Archaean rocks) surrounded by a complex set of Brasiliano–Pan-African (*c.* 600–500 Ma) fold belts (e.g. Trompette, 1997) that formed during assembly of Western Gondwana (Fig. 1). The area of Rio de Janeiro is situated in the Ribeira belt [for recent overviews see Campos Neto (2000), Heilbron *et al.* (2000) and Trouw *et al.* (2000)], which roughly follows the NE–SW-oriented coastline (Fig. 2a) and formed in response to the convergence of the São Francisco and Congo Cratons during closure of the Adamastor Ocean (Vauchez *et al.*, 1994; Alkmim *et al.*, 2001). The continuation of the Ribeira belt towards the north is called the Araçuaí belt (Trompette, 1997; Pedrosa-Soares *et al.*, 2001), which exposes west- to NW-verging thrusts and folds that fringe the São Francisco Craton. Radiometric dating of metamorphic and igneous rocks from the Ribeira belt indicates that they were deformed by the Brasiliano orogeny between 600 and 500 Ma (Machado *et al.*, 1996; Brueckner *et al.*, 2000; Silva, 2001; Heilbron & Machado, 2003). Three pulses of plutonism, two syn-collisional (591–565 Ma and 555–525 Ma) and one post-collisional (*c.* 500 Ma) intrude the metamorphic rocks of both the Araçuaí and the Ribeira belts (Machado *et al.*, 1996; Brueckner *et al.*, 2000).

The Ribeira belt is made up of two terranes (Fig. 2a), the Occidental and Oriental Terranes, subdivided into a number of domains, identified by their contrasting lithology, isotope geochemistry and geochronology (Heilbron *et al.*, 2000). Both the Occidental and Oriental Terranes consist largely of granulite-facies gneisses and charnockites that are markedly different from the predominantly amphibolite-facies rocks from the Araçuaí belt. The various units were juxtaposed at *c.* 595 Ma in the NW and *c.* 500 Ma in the SE (Cabo Frio Domain, Schmitt *et al.*, 1999) during several successive periods of Neoproterozoic

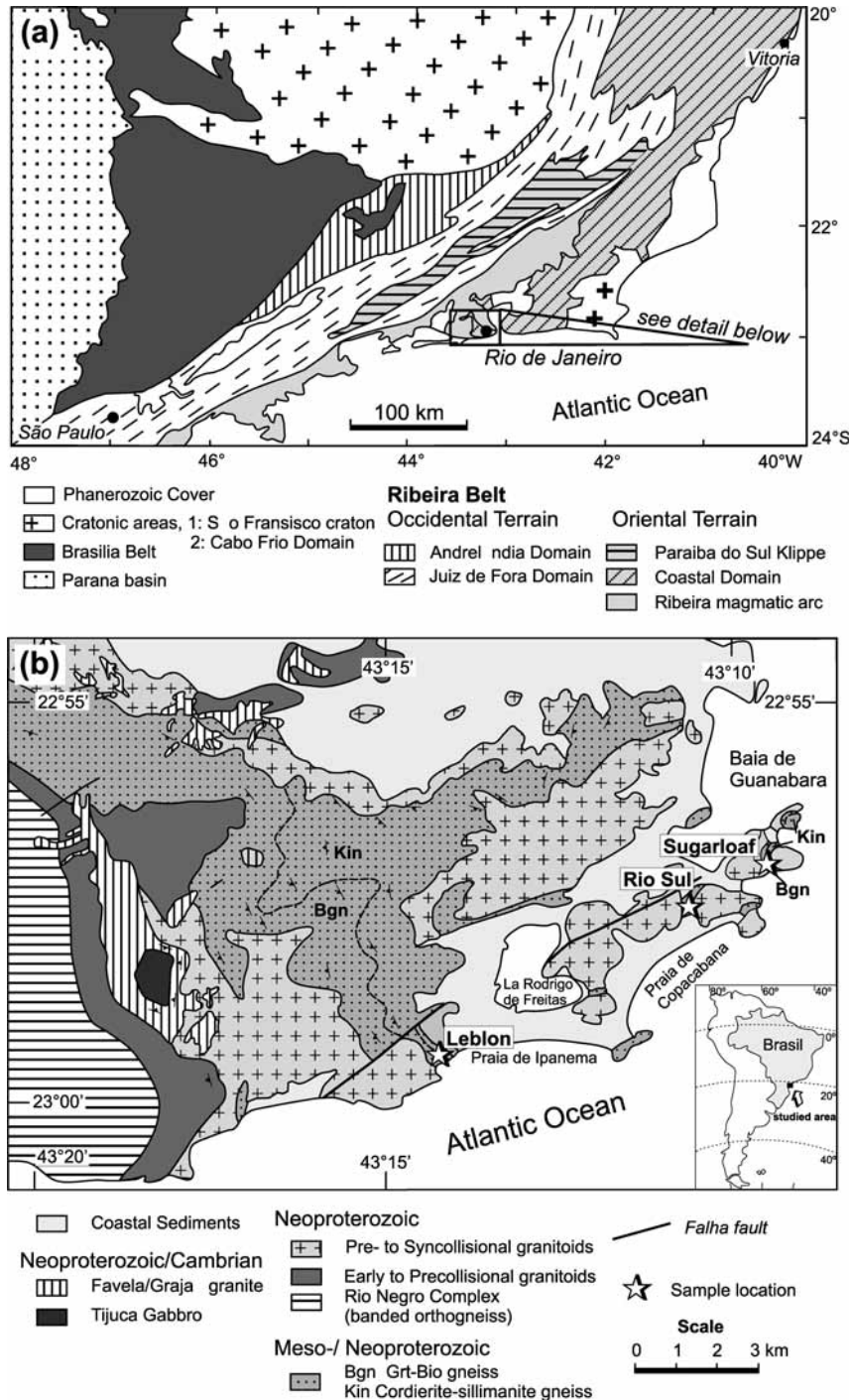


Fig. 2. (a) Tectonic sketch map of the Ribeira belt in SE Brazil, redrawn and modified after Heilbron *et al.* (2000). (b) Simplified geological map of the municipal area of Rio de Janeiro showing the sample locations at Leblon and the Rio Sul Shopping Centre [modified after Helmbold *et al.* (1964) and Heilbron *et al.* (1993)].

orogeny (Machado *et al.*, 1996; Campos Neto, 2000). The Ribeira belt is intruded by pre-collisional calc-alkaline granitoids (Rio Negro granitoids) defining a Brasiliano magmatic arc within the Oriental Terrane (Heilbron *et al.*, 2000).

The kinzigites (garnet–biotite–sillimanite–cordierite granulites) from the Rio de Janeiro area are part of the Coastal Domain within the Oriental Terrane (Heilbron *et al.*, 2000). This region is made of high-grade meta-sedimentary, metaigneous and igneous units with

Table 1: Petrographic description of the investigated samples

Sample location; sample no.	Pl	Kfs	Btl	Btll	Grt	Crd	Crd + Qtz	Sill	Qtz	Cpx	Chl	Accessories
<i>Rio Sul Shopping Centre, Morro de Babilônia</i>												
Rio-A1	x	x	x	x	x	x	x	x	x			Ilm, Rt, Ap
Rio-A2	x		x		x				x	x		Ap, Ttn
Rio-A3	x	x	x	x	x	x		x	x			Ilm, Rt, Ap
<i>Avenida Niemayer, western end of Leblon</i>												
Rio-M688	x	x	x		x	x			x		x	Ilm, Ap
Rio-M280	x	x	x		x	x			x		x	
<i>Close to Sugarloaf</i>												
Rio-K1	x	x	x	x	x	x	x	x	x			Ilm, Rt, Ap

crystallization and metamorphic ages in the range 590–550 Ma (Machado *et al.*, 1996; Heilbron & Machado, 2003). Granitoid plutons (multiple tonalitic to granodioritic bodies) are common in the Rio de Janeiro municipal area and form prominent peaks and landmarks (Fig. 2b). Samples of sillimanite–cordierite-bearing granulites (kinzigites) and related rocks were collected at two outcrops (Avenida Niemayer at the western end of Leblon, and an abandoned quarry in the ‘Morro da Babilônia’ (Babilônia Hill), behind the Rio Sul Shopping Centre in Botafogo, all situated within the municipal area of Rio de Janeiro (Fig. 2b, Table 1).

PETROGRAPHY

The granulite-facies gneisses in the Rio de Janeiro municipal area comprise two types of rocks with sedimentary precursors: (1) highly deformed kinzigites with typical low-*P* granulite-facies assemblages, which form the principal focus of this paper; (2) low-strain granulites and granulofels that are briefly discussed at the end of this section.

Kinzigites (coarse-grained sillimanite–cordierite-bearing granulites)

These deformed, stromatic rocks comprise biotite-rich mesosomes and leucosomes that contain large garnet porphyroblasts up to 1.5 cm in size (samples Rio-A1, Rio-A3, Rio-M688; see Table 1). The stromatic texture is defined by biotite that envelops large garnet porphyroblasts and deformed leucosomes (Fig. 3). Biotite is commonly found in the pressure shadows of the garnet porphyroblasts (Fig. 4a). The leucosomes form wing-like structures around garnet (Fig. 3), are rich in coarse-grained quartz, plagioclase, alkali feldspar and cordierite, and contain minor biotite. Cordierite in the leucosome forms large grains up to 3–4 mm in length. The garnets are often poikiloblastic or relict and contain numerous

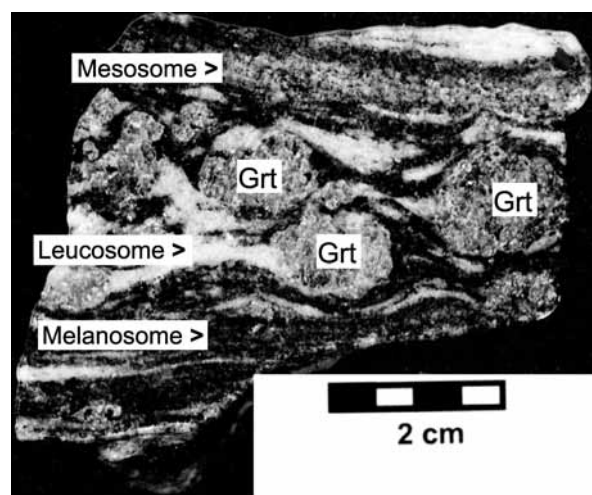


Fig. 3. Sample showing the stromatic texture of the mesosome and melanosome (biotite-rich seams) and the occurrence of large garnet porphyroblasts associated with wing-like leucosome (sample Rio-K1).

inclusions of biotite, ilmenite and Fe-sulphides as well as lobate quartz and plagioclase.

Partial resorption of garnet in the leucosome is common and gives rise to a variety of replacement textures. Initial garnet breakdown is characterized by embayment structures (Fig. 4b) along the outer rims of garnet crystals, where cordierite partly replaces garnet. Cordierite often forms a more or less continuous rim of smaller grains and grain aggregates around garnet and separates it from neighbouring biotite and the leucosome. These cordierite rims may be up to several millimetres thick. In more advanced stages of garnet breakdown, garnet has an atoll-like texture (Fig. 4c), comprising a central core area consisting of cordierite, quartz, biotite–plagioclase symplectites and ilmenite. In these stages of retrogressive garnet breakdown, cordierite grows in symplectitic intergrowth with quartz (Fig. 5a and b). These zones are 500–1000 μm thick and consist of 75–80% cordierite;

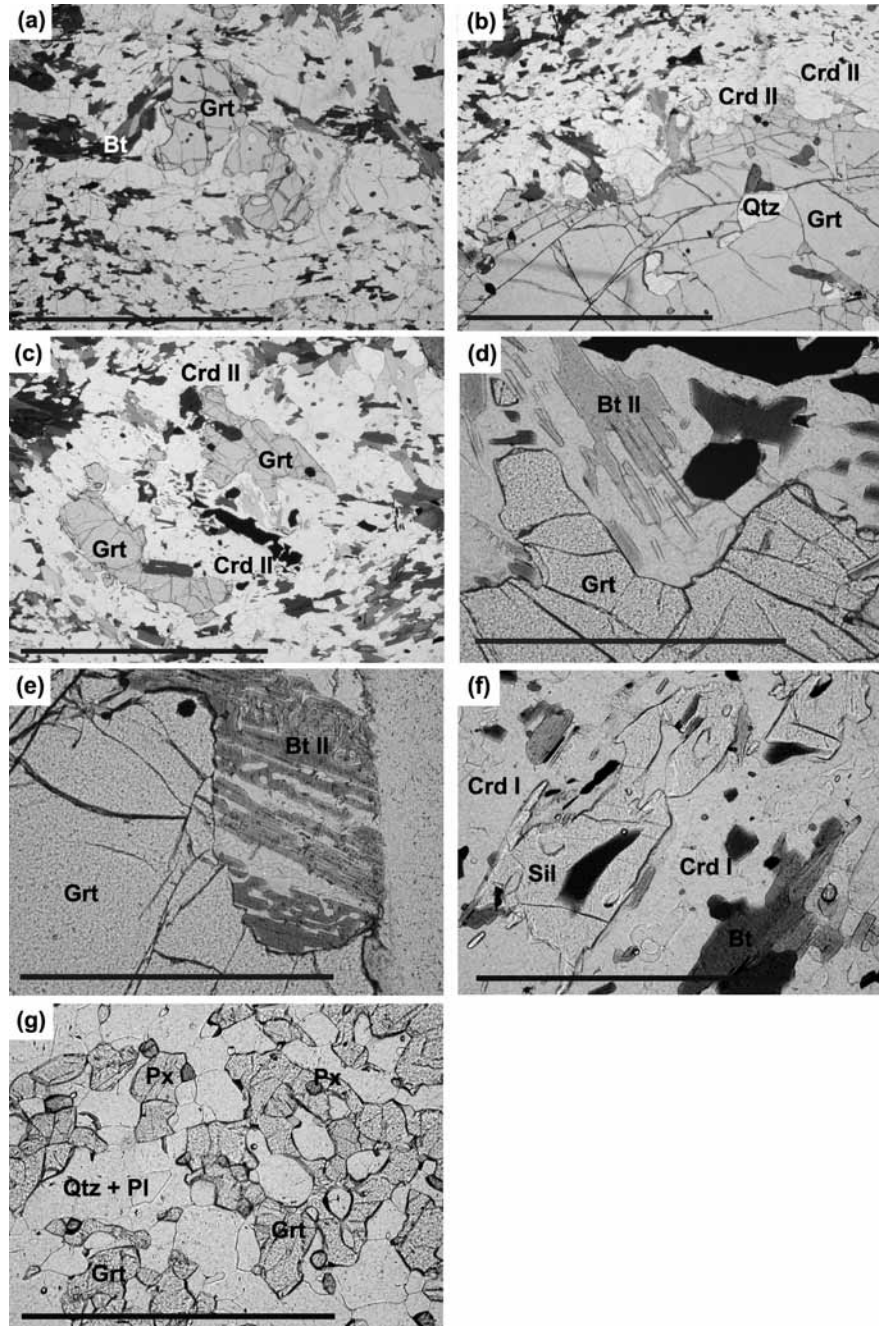


Fig. 4. Photomicrographs from the Rio de Janeiro granulites. (a) Biotite in the pressure shadow of a garnet porphyroblast (Rio-K1); scale bar represents 4 mm; plane-polarized light (ppl). (b) Embayment structures in garnet rim, formation of cordierite (Rio-A1); scale bar represents 4 mm; ppl. (c) Atoll-like garnet, rim of cordierite, biotite in pressure shadow (Rio-A3); scale bar represents 4 mm; ppl. (d) Biotite-quartz intergrowth at the margin of garnet (Rio-A1); scale bar represents 1 mm; ppl. (e) Biotite-quartz-plagioclase intergrowth at the interface between garnet and K-feldspar (Rio-A3); scale bar represents 1 mm; ppl. (f) Sillimanite inclusion in cordierite from the melanosome (Rio-A3); scale bar represents 1 mm; ppl. (g) Granoblastic texture in Cpx-Grt-bearing granulites (Rio-A2); scale bar represents 1 mm; ppl.

quartz accounts for only 20–25% of the symplectite volume. Quartz typically occurs as irregular worm-like bands of 20–25 μm thickness and 100–150 μm length within the cordierite. Volumetric relationships between the phases in the coronas have been obtained by point

counting of backscattered electron images. Cordierite adjacent to garnet often shows late-stage alteration to brownish chlorite growing perpendicular to the garnet-cordierite interface. Symplectitic or skeletal laminar intergrowth of biotite with quartz and plagioclase parallel

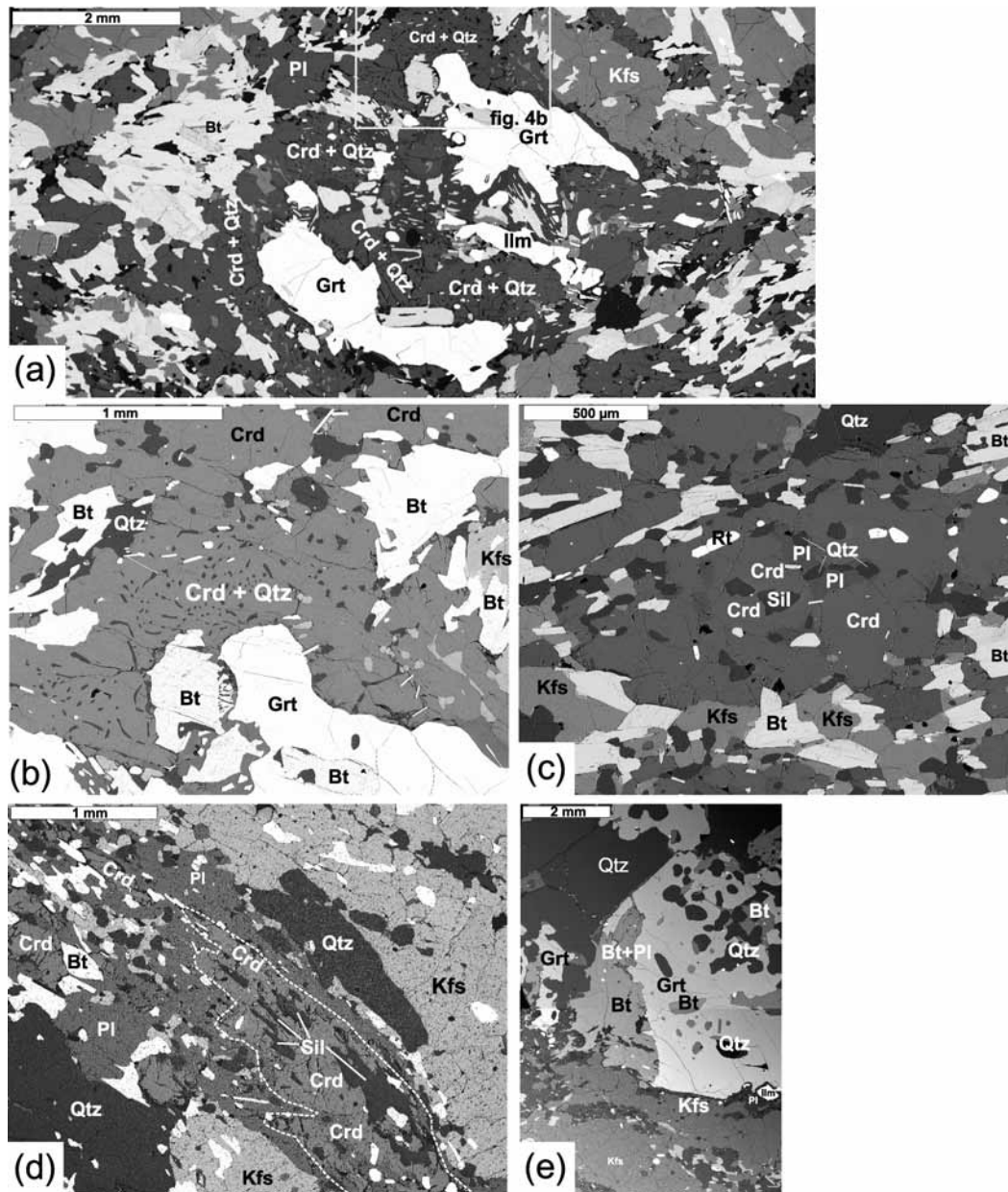


Fig. 5. Backscattered electron images of metamorphic textures. (a) Relic garnet (atoll-like occurrence) also shown in Fig. 4c. Within the core area and along the rim the garnet is replaced by cordierite and quartz. The biotite, formed in the former pressure shadow, is still visible, giving an impression of the original garnet shape; sample Rio-A3. (b) Enlargement of (a) showing the ~0.5 mm thick corona of cordierite and quartz formed during garnet consumption. (c) Sillimanite as small remnants enclosed by cordierite; sample Rio-A1. (d) Sillimanite needles enclosed in cordierite in the melanosome; sample Rio-K1. The boundary between cordierite and the surrounding plagioclase is indicated by the white dashed line. (e) The preservation of a garnet porphyroblast in contact with biotite in its pressure shadow; sample Rio-A3.

to biotite basal planes is relatively common and occurs typically in embayments and inclusions in garnet (Fig. 4d) or inclusions within garnet (Fig. 4e), often where garnet is in contact with K-feldspar (Fig. 4d). The typical laminar spacing between the two phases varies between 20 and 60 μm .

Not all garnet has reaction textures. Some grains, even in thin sections that contain retrogressed garnet,

completely preserve their shape (Fig. 5e). These garnet grains are generally those that are not completely surrounded by leucosomes, remain in contact with biotite in the mesosome, and lack any signs of resorption or other indicators of retrograde mineral reactions.

The mesosome contains biotite, cordierite, plagioclase, K-feldspar, quartz and remnants of sillimanite. Accessory minerals are zircon, apatite, ilmenite, rutile

and Fe-sulphides. Biotite in the mesosome is smaller than biotite formed in the garnet pressure shadows. Cordierite encloses elongated sillimanite (Figs 4f and 5c, d) and usually exceeds the sillimanite volume significantly. Remnant sillimanite may carry small inclusions of biotite. However, in some places sillimanite remains in contact with plagioclase. Whereas K-feldspar in the leucosome occurs as large, millimetre-sized crystals, K-feldspar in the mesosome is much smaller in grain size and occurs in equilibrium with both biotite and quartz.

Granofels/low-strain granulites

The granofels has a layering of biotite-rich layers, plagioclase–quartz-rich layers and layers with the assemblage plagioclase–clinopyroxene–garnet–titanite and quartz. It shows no obvious indication for partial melting. The foliation is parallel to the compositional layering and is defined by biotite. In contrast to the kinzigites, these rocks have an equigranular and polygonal fabric in both the biotite- and clinopyroxene-bearing layers (Fig. 4g). However, garnet occurs as anhedral, amoeboid and inclusion-rich porphyroblasts overgrowing the polygonal texture. Garnet is mainly found in leucocratic plagioclase–quartz layers and in the boundary zone between leucocratic layers and the layers bearing biotite or pyroxene.

MINERAL CHEMISTRY

Mineral compositions were analysed with a JEOL JSM 6310 secondary electron microscope equipped with an energy dispersive (EDS) system combined with a wavelength-dispersive (WDS) spectrometer at the Institute of Mineralogy and Petrology, University of Graz. Operating conditions were 15 kV accelerating voltage, a beam current of 15 nA and counting times of 100 s (EDS) and 20 s (WDS). Analyses were corrected for absorption, atomic number and fluorescence using the Phi-Rho-Z correction procedure. Natural and synthetic standards were used for calibration. Reported X_{Mg} values in biotite, clinopyroxene and cordierite represent $Mg/(Mg + Fe)$; in garnet X_{Alm} is defined as $Fe^{2+}/(Fe^{2+} + Mg + Mn + Ca)$. Reported values for X_{Prp} and X_{Sps} are calculated in a corresponding way for Mg and Mn; X_{Andr} represents $Fe^{3+}/(Al^{VI} + Cr + Fe^{3+} + Ti)$, and X_{Grs} represents $[Ca/(Fe^{2+} + Mg + Mn + Ca)] - X_{Andr}$. Representative mineral analyses are given in Tables 2 and 3.

Garnet

In the kinzigites, the garnet composition (Table 2) is dominated by almandine ($X_{Alm} = 0.61–0.73$) followed by pyrope ($X_{Prp} = 0.21–0.35$), and minor grossular ($X_{Grs} = 0.03$) and spessartine ($X_{Sps} = 0.02–0.03$). Core

compositions tend towards higher pyrope and lower almandine contents compared with the rim compositions. Compositional zoning is more pronounced in the larger garnet porphyroblasts (grain size $\gg 2$ mm; see Fig. 6). Smaller grains (< 1.5 mm) or grains that show extensive reaction textures (reaction to cordierite–quartz intergrowths) display less pronounced chemical variations between core ($X_{Alm} = 0.68$ and $X_{Prp} = 0.25$) and rim ($X_{Alm} = 0.72$, $X_{Prp} = 0.21$; Fig. 6). The core compositions of these small garnet grains are similar to the rim compositions from the larger garnet grains in which a more pronounced chemical zoning can be observed.

In the weakly deformed granulites (granofels), the composition of amoeboid garnet varies depending on its textural position within clinopyroxene- or biotite-bearing layers. In the clinopyroxene-bearing layers, garnet is rich in CaO and MnO with a typical composition dominated by the almandine ($X_{Alm} = 0.51$), grossular ($X_{Grs} = 0.21$) and spessartine ($X_{Sps} = 0.17$) components. These garnets have low pyrope contents not exceeding $X_{Prp} = 0.10$. In the biotite-bearing layers garnets are unzoned, Fe-, Mg-rich and low in Ca and Mn, with a typical chemical composition of $X_{Alm} = 0.68$, $X_{Grs} = 0.05$, $X_{Prp} = 0.22$ and $X_{Sps} = 0.04$. Garnet occurring in leucocratic layers lacking both biotite and clinopyroxene has an intermediate composition between the Mn-, Ca-rich and Mn-, Ca-poor garnet compositions as indicated above.

Biotite

In the kinzigites three types of biotite can be distinguished based on their textural occurrence: biotite in the mesosome, biotite in pressure shadows around garnet, and biotite as inclusions in garnet porphyroblasts. Biotite in the mesosome is low in X_{Mg} (0.53–0.57). The X_{Mg} is higher where biotite is in contact with garnet or occurs as inclusions in garnet (0.58–0.75). Biotite inclusions in garnet have higher Ti contents (> 0.3 cations p.f.u.) and narrower compositional variations with respect to X_{Mg} (0.67–0.68).

In the fine-grained granulites (granofels), biotite composition varies according to its textural occurrence. Biotite close to garnet has high X_{Mg} values of 0.69–0.75 and low Ti contents, whereas biotite in garnet-free layers has lower X_{Mg} (0.61) and higher Ti contents (up to 5.23 wt %, or 0.3 atoms p.f.u.).

Cordierite

Cordierite is highly magnesian, ranging in X_{Mg} between 0.72 and 0.80 (Table 3). Despite this spread in composition the X_{Mg} in any particular sample is much narrower and only varies by 0.02. No chemical differences in cordierite composition were detected between cordierite that is part of the coarse-grained assemblage and cordierite coronas on garnet. Similarly, no zoning with respect to the Mg and Fe content could be detected

Table 2: Representative mineral compositions for cordierite and garnet from the kinzigites and granofels

	Cordierite				Garnet						
	Rio-A1 matrix	Rio-A3 Grt contact	Rio-K1 matrix	Rio-K1 leucosome	Rio-A1 Rim	Rio-A1 Core	Rio-A2 Bt zone	Rio-A2 Cpx zone	Rio-A3 rim	Rio-K1 rim	
SiO ₂	49.50	49.19	49.31	48.89	SiO ₂	38.55	39.10	38.30	37.71	38.38	38.44
TiO ₂	0.00	0.01	0.01	0.00	TiO ₂	0.00	0.00	0.12	0.08	0.00	0.04
Al ₂ O ₃	32.90	32.66	32.38	32.29	Al ₂ O ₃	20.94	21.25	21.02	20.93	21.28	21.30
Fe ₂ O ₃	0.33	0.63	0.00	0.00	FeO	31.44	29.13	23.48	29.78	32.19	31.90
FeO	6.20	6.20	6.53	6.46	MnO	1.18	0.91	7.83	1.54	1.39	0.92
MnO	0.04	0.07	0.06	0.04	MgO	6.80	9.05	2.32	6.14	5.67	7.10
MgO	9.56	9.74	9.42	9.42	CaO	0.97	0.89	7.99	1.87	1.10	1.20
CaO	0.08	0.00	0.01	0.07	Total	99.88	100.33	101.08	98.05	100.01	100.90
Na ₂ O	0.08	0.00	0.12	0.00	<i>Normalized to 16 cations</i>						
K ₂ O	0.04	0.00	0.00	0.02	Si	6.07	6.03	6.04	6.05	6.07	5.98
Total	98.73	98.51	97.84	97.19	Al ^{IV}	0.00	0.00	0.00	0.00	0.00	0.02
<i>Normalized to 18 oxygens and 11 cations</i>					Al ^{VI}	3.88	3.86	3.91	3.95	3.97	3.88
Si	5.03	5.01	5.06	5.05	Fe ³⁺	0.00	0.07	0.00	0.00	0.00	0.13
Ti	0.00	0.00	0.00	0.00	Ti	0.00	0.00	0.01	0.01	0.00	0.00
Al	3.94	3.92	3.91	3.93	Mg	1.59	2.08	0.55	1.47	1.34	1.65
Fe ³⁺	0.03	0.05	0.00	0.00	Fe ²⁺	4.14	3.68	3.10	3.99	4.26	4.02
Fe ²⁺	0.53	0.53	0.56	0.56	Mn	0.16	0.12	1.05	0.21	0.19	0.12
Mn	0.00	0.01	0.01	0.00	Ca	0.16	0.15	1.35	0.32	0.19	0.20
Mg	1.45	1.48	1.44	1.45	Almandine	68.35	61.08	51.28	66.65	71.35	67.12
Ca	0.01	0.00	0.00	0.00	Andradite	0.00	1.86	0.00	0.00	0.00	3.30
Na	0.02	0.00	0.02	0.01	Grossular	2.70	0.58	22.36	5.36	3.12	0.04
K	0.01	0.00	0.00	0.00	Pyrope	26.35	34.51	9.03	24.50	22.41	27.51
X _{Mg}	0.73	0.74	0.72	0.72	Spessartine	2.60	1.97	17.32	3.49	3.12	2.03

in the coronas around garnet, where cordierite forms the major phase. Analytical totals between 97.0 and 99.7 wt % suggest the presence of varying amounts of channelled H₂O–CO₂ fluids in the cordierite lattice.

Plagioclase

Plagioclase in the mesosome is andesine ($X_{An} = 0.29$ – 0.49 ; Table 3). The compositional variations are due to subtle differences in bulk composition between the investigated samples. In the leucosome the plagioclase is richer in Ca, reaching $X_{An} > 0.5$. In the granofels (sample Rio-A2) feldspar composition varies between garnet-bearing and garnet-free layers. Whereas feldspars in the non-garnet-bearing layers are homogeneous in composition with $X_{An} = 0.46$, feldspars in the biotite-rich and clinopyroxene-rich layers appear more complex in composition. In feldspars close to garnet a pronounced zoning could be detected, with cores comprising albite-rich compositions ($X_{Ab} = 0.43$, $X_{An} = 0.57$) and rims much higher in anorthite component ($X_{Ab} = 0.7$ – 0.15 and

$X_{An} = 0.85$ – 0.93). However, most of the feldspars are rich in the anorthite component.

Clinopyroxene

Clinopyroxene is a common mineral phase in anhydrous layers of the granofels. The analysed clinopyroxenes are predominantly diopside or hedenbergite with X_{Mg} varying between 0.57 and 0.49 and low (<1 wt %) Al₂O₃ contents (Table 3). Clinopyroxene contains up to 1.6 wt % MnO (corresponding to 0.05 atoms p.f.u.).

INTERPRETATION OF MICROTEXTURES AND REACTION HISTORY

The mineral assemblages described above may be interpreted in terms of several equilibrium parageneses. The earliest assemblage is that recorded by the fabric in the mesosomes, and is also partly preserved as inclusions in

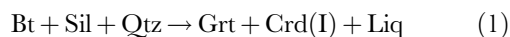
Table 3: Representative mineral compositions for biotite, clinopyroxene and plagioclase from the kinzigites and granofels

Biotite							Clinopyroxene			Plagioclase		
Rio-A1 incl. in Grt	Rio-A1 melanosome	Rio-K1 melanosome	Rio-A2 Grt zone	Rio-A2 Grt-free zone	Rio-A3 bio16	Rio-A2 Cpx3a	Rio-A2 Cpx4b	Rio-A1 pl28a	Rio-A3 pl3			
SiO ₂	35-22	35-64	34-93	36-95	36-57	36-78	SiO ₂	52-10	51-73	SiO ₂	61-10	60-80
TiO ₂	5-84	5-97	6-46	3-12	5-03	5-72	TiO ₂	0-13	0-16	TiO ₂	0-00	0-00
Al ₂ O ₃	16-67	15-78	15-69	16-36	15-42	16-65	Al ₂ O ₃	0-90	1-03	Al ₂ O ₃	23-93	24-13
Fe ₂ O ₃	0-00	0-00	0-00	0-00	0-00	0-00	MgO	10-26	8-73	MgO	0-00	0-00
FeO	12-72	16-26	16-29	11-77	14-02	13-78	FeO	13-84	15-91	FeO	0-03	0-00
MnO	0-00	0-07	0-02	0-00	0-06	0-00	MnO	1-51	1-62	CaO	6-01	6-08
MgO	13-92	10-78	11-08	14-94	12-40	13-03	NiO	0-00	0-00	Na ₂ O	7-69	8-17
CaO	0-00	0-03	0-00	0-07	0-08	0-00	CaO	20-88	21-47	K ₂ O	0-23	0-17
Na ₂ O	0-32	0-11	0-14	0-00	0-00	0-29	Na ₂ O	0-14	0-14	Total	98-99	99-35
K ₂ O	9-31	9-74	9-92	9-62	9-74	9-66	K ₂ O	0-01	0-00	<i>Normalized to 8 oxygens</i>		
Total	94-01	94-39	94-54	92-83	93-32	95-91	Total	99-80	100-78	Si	2-74	2-72
<i>Normalized to 11 cations</i>							<i>Normalized to 4 cations</i>			Al	1-26	1-27
Si	2-65	2-72	2-67	2-79	2-78	2-72	Si	2-00	1-99	Ti	0-00	0-00
Ti	0-33	0-34	0-37	0-18	0-29	0-32	Ti	0-00	0-00	Fe ³⁺	0-00	0-00
Al	1-48	1-42	1-41	1-45	1-38	1-28	Al	0-04	0-05	Mg	0-00	0-00
Fe ³⁺	0-00	0-00	0-00	0-00	0-00	0-00	Fe	0-44	0-51	Mn	0-00	0-00
Fe ²⁺	0-80	1-04	1-04	0-74	0-89	0-85	Mn	0-05	0-05	Ca	0-29	0-29
Mn	0-00	0-01	0-00	0-00	0-00	0-00	Mg	0-59	0-50	Na	0-67	0-71
Mg	1-56	1-23	1-26	1-68	1-41	1-43	Ni	0-00	0-00	K	0-01	0-01
Ca	0-00	0-00	0-00	0-01	0-01	0-00	Ca	0-86	0-88	X _{An}	29-74	29-13
Na	0-05	0-02	0-02	0-00	0-00	0-04	Na	0-01	0-01	X _{Ab}	68-90	70-19
K	0-89	0-95	0-97	0-93	0-95	0-91	K	0-00	0-00	X _{Or}	1-36	0-96
X _{Mg}	0-66	0-54	0-55	0-69	0-61	0-63	X _{Mg}	0-57	0-49			

garnet. This assemblage involves the phases Bt + Sil + Kfs + Pl + Qtz and accessories [abbreviations after Kretz (1983)] and we refer to this assemblage as M_1 . The assemblage preserves the earliest foliation developed during D_1 . However, even in the mesosomes, this assemblage is overgrown by a coarse-grained later assemblage involving cordierite.

Prograde evolution and peak metamorphic assemblages

Mineral textures in the kinzigites reflect the instability of the M_1 mineral assemblage in both the mesosomes and the leucosomes to form the coarse-grained peak metamorphic paragenesis. In the leucosomes, the M_1 paragenesis is preserved only as inclusions in garnet. We interpret the coarse-grained peak assemblage in the leucosomes to have formed from M_1 in response to the incongruent KFMASH melting net-reaction



and suggest that the remnant biotite in the leucosomes is evidence for modal excess of biotite over sillimanite in the stoichiometry of this reaction. It should be noted that we use the term ‘net-reaction’ for petrographically observed growth and breakdown textures and not for stoichiometrically balanced reactions; also, that this reaction forms garnet and melt plus the first generation of coarse-grained cordierite(I) in the leucosomes. This assemblage is the coarsest-grained peak paragenesis observed in the rocks. We consequently interpret it to reflect peak conditions and refer to it as M_2 .

In the mesosomes the major mineral reaction observed during M_2 is the formation of coarse-grained cordierite overgrowths on sillimanite in response to the inferred net-reaction



We interpret the M_2 assemblage in the mesosomes to consist of Bt + Crd + Pl + Kfs + Qtz. However, we acknowledge the fact that the mesosomes probably

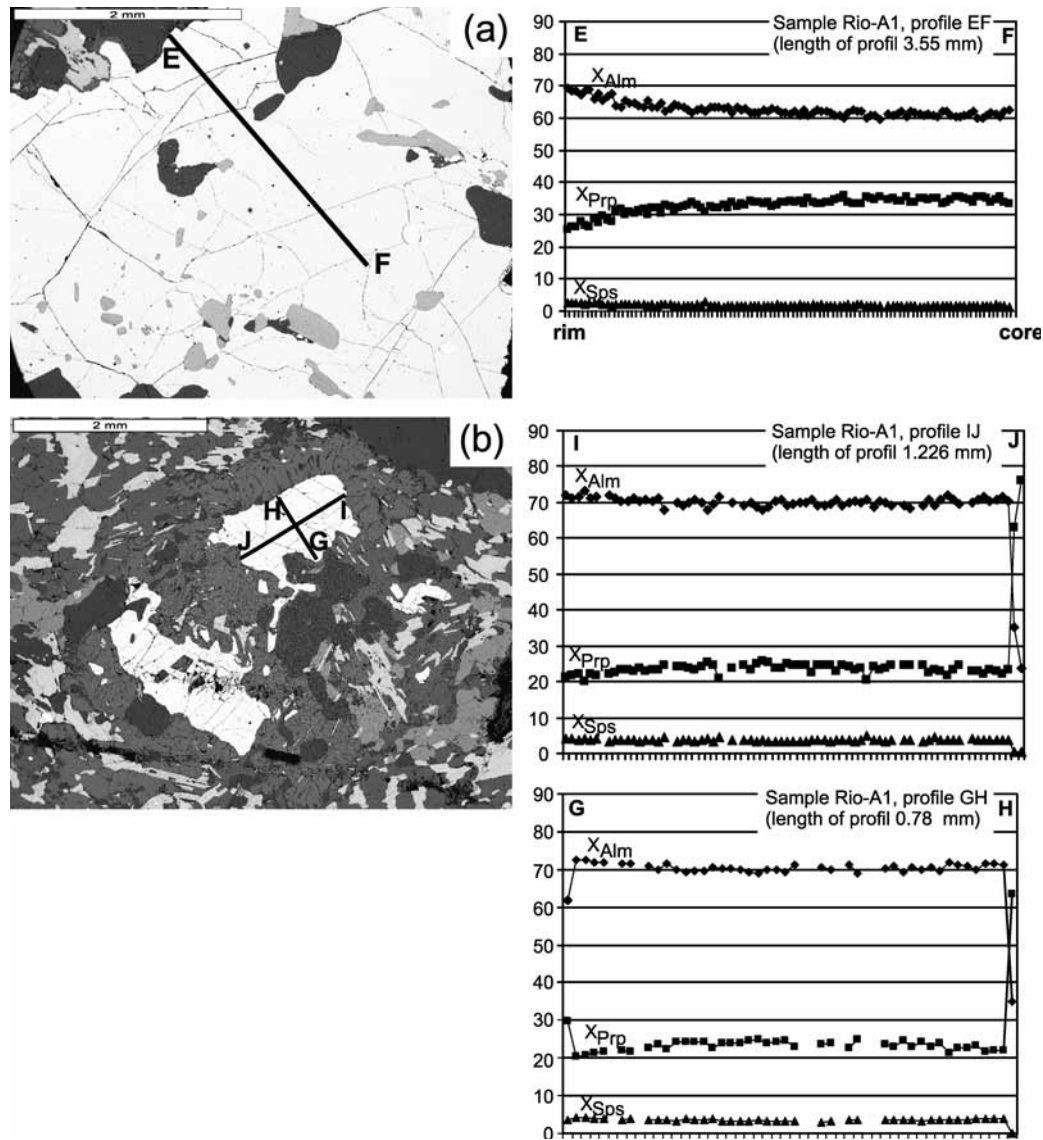


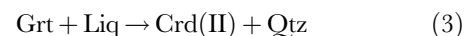
Fig. 6. Compositional zoning profiles and backscattered electron images of (a) a large garnet porphyroblast in contact with leucosome and (b) remnants of garnet surrounded by a corona of cordierite and quartz; sample Rio-A3.

represent melt-depleted restitic material formed during the partial melting event. Thus, the M_2 equilibrium assemblage probably includes both the melanosome and the leucosome assemblages but it is distinguished from M_1 by the growth of cordierite. It should be noted that the preservation of biotite–sillimanite equilibria in the presence of garnet–cordierite parageneses is not possible in the system KFMASH, but forms no contradiction in the more realistic Na_2O – CaO –KFMASH system (e.g. White & Powell, 2002).

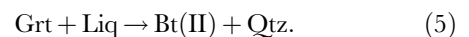
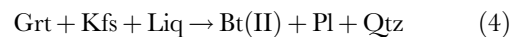
Retrogression and symplectite formation

Symplectites of cordierite and quartz coronas that enclose garnet are inferred to have grown in response to

the inferred net-reaction



which causes the separation of garnet from biotite by cordierite coronas. It also leaves behind remnants of garnet. In other places, secondary biotite is formed as a result of the inferred net-reaction



Biotite(II) forms skeletal intergrowths with quartz and/or plagioclase. This paragenesis is referred to as M_3 . The formation of assemblage M_3 is highly localized and

suggests that the equilibrium volumes during M_3 were much smaller than those that accompanied peak conditions. Several garnet grains enclosed in the leucosome are still in contact with the biotite that formed in pressure shadows (Fig. 5e).

In summary, the P – T evolution of the Rio de Janeiro sillimanite–cordierite-bearing granulites is characterized by a reaction sequence that can be described in a two-stage development. The first stage involves the production of partial melt, together with cordierite(I) and garnet growth during M_2 . This event is the metamorphic peak. It is emphasized that the assemblage here referred to as M_1 is unlikely to characterize an event of its own and is defined only on the basis of the relic evidence for parageneses from the prograde path towards M_2 . The second stage involves garnet consumption during M_3 together with the formation of cordierite(II).

CONVENTIONAL THERMOBAROMETRY AND AVERAGE P – T DETERMINATION

Representative mineral pairs from various samples were selected to estimate P – T conditions that accompanied the metamorphic evolution of the parageneses. The results are summarized in Table 5. For garnet–biotite pairs in contact (biotite inclusions in garnet are interpreted to be formed or re-equilibrated during garnet growth and melting of the rocks) from the kinzigites (sample Rio-A1) metamorphic temperatures of 712°C (Ferry & Spear, 1978) and 723°C (Hodges & Spear, 1982) could be estimated. Applying the calibrations by Perchuk & Lavrent'eva (1983) and Bhattacharya *et al.* (1992) to the same mineral pairs, lower temperatures of 653°C and 649°C were calculated.

In the granofels (fine-grained granulites, sample Rio-A2) biotite + garnet- and clinopyroxene + garnet-bearing layers together with coexisting plagioclase and quartz allow the calculation of metamorphic conditions by applying different calibrations of the biotite–garnet thermometer, the clinopyroxene–garnet thermometer, the garnet–clinopyroxene–plagioclase barometer (Powell & Holland, 1988) and the clinopyroxene–plagioclase–quartz barometer (Ghent *et al.*, 1987). Whereas clinopyroxene–garnet thermometry (Ellis & Green, 1979; Powell, 1985; Krogh, 1988; Krogh–Ravna, 2000) gives $T = 690$ – 732 °C, temperatures calculated using the Fe–Mg exchange between biotite and garnet scatter largely between 590°C and 738°C. The higher temperatures are obtained by using garnet–clinopyroxene and garnet–biotite core compositions of minerals that are not in direct contact with each other, thus avoiding the effect of post-peak inter-crystalline diffusion. The large spread in temperatures might be a result of a later growth

episode of garnet, overgrowing older biotite, but not reaching equilibrium conditions. Pressure estimates calculated by applying the above-mentioned calibrations yield $P = 4$ – 5 kbar assuming $T = 700$ °C.

From the breakdown reaction of garnet to cordierite(II) and quartz [reaction (3)] metamorphic temperatures of 608–678°C were calculated using the calibration of the Grt–Crd Fe–Mg exchange thermometer by Perchuk & Lavrent'eva (1983) applied to the rim composition of garnet and the newly formed cordierite.

P – T estimates for each sample were made using multi-equilibria calculations and the Holland & Powell dataset [average P – T mode, THERMOCALC version 3.21 and the dataset of Holland & Powell (1998; 1999 update)]. End-member activities used in the calculations have been calculated using the program AX (available at <http://www.esc.cam.ac.uk/staff/holland/ax.html>). In our approach we used biotite–garnet(rim)–cordierite–plagioclase–quartz–sillimanite–H₂O assemblages from samples Rio-A1, Rio-A3 and Rio-K1. Results of the average P – T calculations for three samples (Table 6) agree within error, giving $T = 690 \pm 84$ °C to 740 ± 84 °C and $P = 5.8 \pm 0.9$ kbar to 6.5 ± 0.9 kbar. These results were calculated assuming H₂O-present conditions. Assuming lower H₂O activities ($a_{\text{H}_2\text{O}} = 0.5$ and 0.2) does not lead to appreciably lower metamorphic temperatures (calculated conditions are 10–16°C lower than those reported for $a_{\text{H}_2\text{O}} = 1$). Calculated error estimates for the various H₂O activities are equally high in the range of ± 84 °C as obtained for H₂O-present conditions, and calculated pressures are 0.7 kbar and 1.3 kbar lower than those calculated for the high water activities. When garnet core composition were combined with matrix biotite, plagioclase and K-feldspar compositions, incomplete sets of independent reactions resulted in unrealistically high-grade conditions of $T > 900$ °C and $P \approx 7.4$ kbar assuming $a_{\text{H}_2\text{O}} = 1$. More realistic conditions were calculated assuming lower H₂O activities of 0.5 and 0.2. These gave formation conditions of $T = 851 \pm 54$ °C, $P = 6.5 \pm 1.6$ kbar and $T = 753 \pm 45$ °C, $P = 5.5 \pm 1.5$ kbar, respectively. Because of the difficulties in clearly defining mineral phases in both chemical and textural equilibrium these results can only be interpreted as an estimate for the conditions during M_2 and/or M_3 .

MODELLING OF PHASE RELATIONS: P – T PSEUDOSECTION

To elucidate the P – T evolution of the kinzigites, the effects of P – T changes on stable phase assemblages and the formation of melt were interpreted using P – T pseudosections (Hensen, 1971). Pseudosections are an invaluable aid for interpreting metamorphic reaction textures, as they can be contoured for modal proportions of phases

Table 4: Duplicate major oxide analyses (XRF analyses) of bulk composition of sample Rio-A3 used in the calculation of the P - T pseudosection

Sample	Rio-A3a wt %	Rio-A3a mol %	Rio-A3b wt %	Rio-A3b mol %
SiO ₂ (S)	63.66	69.28	63.37	69.51
TiO ₂	0.90		0.90	
Al ₂ O ₃ (A)	15.46	9.91	15.43	9.97
FeO (F)	10.32	9.39	10.31	9.46
MnO	0.20		0.21	
MgO (M)	3.91	6.34	3.90	6.38
CaO (C)	1.08	1.26	1.08	1.27
Na ₂ O (N)	1.25	1.32	1.20	1.28
K ₂ O (K)	3.06	2.50	3.06	2.14
P ₂ O ₅	0.09		0.09	
Total	99.95	100.00	99.53	100.00
H ₂ O ⁻	0.11		0.10	
LOI	0.01		0.04	
H ₂ O _{tot}	0.12		0.14	

Mol % values are normalized NCKFMAS (anhydrous) compositions.

and compositional isopleths (e.g. Stüwe & Powell, 1995). As such, they provide additional and valuable information about P - T variations on the basis of observed growth and consumption of minerals during metamorphism, although our increasing understanding of equilibration volumes (e.g. Stüwe, 1997) suggests that care must be taken when interpreting reaction textures.

The reaction textures described above were considered by calculating pseudosections in the eight-component model system, Na₂O-CaO-K₂O-FeO-MgO-Al₂O₃-SiO₂-H₂O (NCKFMASH). Bulk compositions of two representative samples were obtained by X-ray fluorescence (XRF) analysis and are listed in Table 4. Normalized to the eight-component model system considered here, the bulk composition of sample Rio-A3 is (in mol %): Na₂O 1.27, CaO 1.21, K₂O 2.05, FeO 9.05, MgO 6.11, Al₂O₃ 9.55, SiO₂ 66.71, H₂O 5. The amount of H₂O (~2 wt %) has been chosen so that complete consumption of H₂O occurs close to the solidus. Phase equilibria calculations were performed using THERMOCALC 3.21 (Powell & Holland, 1988; Powell *et al.*, 1998) and the internally consistent thermodynamic dataset (Holland & Powell, 1998; 1999 update). Phases considered in the calculations were garnet, plagioclase, K-feldspar, cordierite, biotite, orthopyroxene, sillimanite, quartz and a liquid melt phase. The solution model used for silicate melt in NCKFMASH is that presented by

White *et al.* (2001). Coding for all phases, including the solution behaviour of non-ideal solid solutions, follows White *et al.* (2001). Calculations were performed with quartz in excess, as it is observed in all assemblages.

Results of the phase calculations are presented in Figs 7 and 8. In the NCKFMASH system no univariant lines are seen in the considered P - T range of 600–900°C and 3–9 kbar for the chosen bulk composition. Divariant fields are sparse and make up only a very limited area of the P - T pseudosection. The field of highest variance is the hexavariant field involving garnet, plagioclase and melt. The solidus is very steep and generally has a negative slope. It is located in the temperature range between $T = 670^\circ\text{C}$ at $P = 9$ kbar and $T = 705^\circ\text{C}$ at $P = 3$ kbar. On the high-temperature side of the solidus a number of di- to trivariant fields occur across a small T range in which an aqueous fluid is replaced by melt. In Fig. 7b modal contours for melt (mol %) are superimposed on the pseudosection presented in Fig. 7a. The contours are steep and generally have a positive slope in P - T space, except for the melt modes within the trivariant field Bt + Pl + Grt + Crd + Sil + liq (+ Qtz). In this field, which is characterized by the cordierite-out reaction towards higher pressures, lines of constant melt fraction show shallow negative slopes.

From the steep slope of the melt contours in wide parts of the pseudosection it can be inferred that decompression would not lead to significant melting in these rocks; this leaves heating as the most probable cause for partial melting. The suprasolidus part of the pseudosection is characterized by three small divariant fields (1, 2 and 7). Of these, fields 2 and 7 are of special interest as they constrain the P - T range in which the evolution of the investigated rocks must have occurred. The narrow divariant field 2 constrains the position of the reaction producing cordierite at the expense of sillimanite during prograde heating. This satisfactorily explains the textures observed in our samples. For the bulk composition considered the divariant field 7 indicates the formation of orthopyroxene at the expense of biotite. As no orthopyroxene-bearing assemblages are observed, this field is considered as the low-pressure and upper temperature boundary of the P - T conditions relevant for the investigated rocks. Thus the P - T evolution of the investigated rocks is constrained to have crossed field 2, but not to have entered field 7. The observed mineral associations M_1 to M_3 can be assigned to a P - T window of interest from 3.5 to 7.5 kbar and from 750°C to 800°C (Fig. 8) of the calculated P - T pseudosection.

Metamorphic evolution and P - T path

Figure 8 presents a pseudosection based on Fig. 7, contoured for modal proportions of garnet, cordierite and

Table 5: Mineral composition and temperature and pressure estimates of metamorphic conditions of the Rio de Janeiro granulites

Sample	X_{Mg}					X_{An}					Temperature (°C) at estimated pressure of 5/7 kbar				
	Grt	Cpx	Bt	Crd	Pl	Grt—Cpx				Grt—Bt				Grt—Crd	
						E&G '79	P '85	K '88	K '00	F&S '78	H&S '82	P&L '83	B <i>et al.</i> '92		P&L '83
Rio-A1	0.32	—	0.66	—	—						704/712	715/723	648/653	647/649	
	0.27	—	—	0.73	—										678
Rio-A2	0.15	0.58	—	—	0.94	684/690	664/669	636/642	721/732						
	0.17	0.59	—	—	—	698/703	678/683	646/652	741/752						
	0.291	—	0.614	—	—					729/738	751/759	660/665	675/677		
	0.291	—	0.694	—	—					586/594	607/615	587/593	604/606		
	0.291	—	0.612	—	—					732/741	754/763	661/667	677/679		
Rio-A3	0.24	—	—	0.75	—										608
Rio-K1	0.3	—	—	0.76	—										680

Pressure (kbar) at estimated temperatures of 700°C											
Grt—Cpx—Pl—Qtz ¹						Cpx—Pl—Qtz ²					
Rio-A2	0.15	0.58	—	—	0.94	3.5					5.6

E&G '79, Ellis & Green (1979); P '85, Powell (1985); K '88, Krogh (1988); K '00, Krogh-Ravna (2000); F&S '78, Ferry & Spear (1978); H&S '82, Hodges & Spear (1982); P&L '83, Perchuk & Lavrent'eva (1983); B *et al.* '92, Bhattacharya *et al.* (1992).

¹Powell & Holland (1988).

²Ghent *et al.* 1987.

quartz, to discuss the P - T evolution of the investigated rocks. It can be used to infer a metamorphic P - T path by relating the textural changes between the M_1 , M_2 and M_3 assemblages to both topological and modal abundances.

The earliest recognized assemblage (M_1) is characterized by the trivariant field Pl + Bt + Grt + Sil + Kfs + liq (+Qtz). This field is located on the low-temperature side of the narrow divariant field 2, in which sillimanite is replaced by cordierite at $P > 6$ kbar and $T < 800^\circ\text{C}$. The crossing of this narrow divariant field represents the KFMASH univariant reaction Sil + Bt = Grt + Crd (+liq + Qtz + Kfs), which may be considered as the amphibolite-facies to granulite-facies transition (White *et al.*, 2001). The first observed deformation phase D_1 occurred synchronous with the development of this assemblage.

The peak metamorphic assemblage (M_2) is characterized by the trivariant assemblage Pl + Grt + Bt + Crd + Kfs + liq (+Qtz) on the high-temperature side of divariant field 2. This field is stable through the P - T range between $P = 4$ and 7 kbar and $T = 730$ and 820°C (Figs 7 and 8). The P - T position of this field is not particularly

sensitive to the bulk composition, when compared with a P - T pseudosection calculated for an average pelite composition as presented by, for example, White *et al.* (2001). In both the P - T pseudosections presented by White *et al.* (2001) and the present study this field is bordered by small di- and trivariant fields representing sillimanite-in towards higher pressures and orthopyroxene-in towards lower pressures. In principle, the divariant field 2 may be crossed by decompression as well as by heating. However, melt contours in both the M_1 trivariant field and the M_2 trivariant fields are steep. Considering that we observe increased leucosome formation associated with the transition, we suggest heating rather than decompression from M_1 to M_2 as the more likely path. The transition from the M_1 to M_2 assemblage is clearly shown by reaction textures (cordierite growth around sillimanite; see Figs 3g and 4d) indicating the crossing of the narrow divariant field between the two trivariant fields of interest.

The M_3 assemblage is characterized by the same assemblage as the M_2 paragenesis, but by a shift in the volumetric proportions of phases. We therefore rely on modal contours within the trivariant fields of interest to

Table 6: Average P–T calculations for mineral assemblages interpreted to be representative from samples Rio-A1, Rio-A3 (Rio Sul locality) and Rio-K1 (Sugarloaf locality)

Average P–T calculated from sample Rio-A1, pl–grt(rim)–bt–crd–qtz–sill–H ₂ O assemblages													
End-member:	crd	fcrd	py	gr	alm	phl	ann	east	an	q	H ₂ O	sill	
Activity (a):	0.550	0.0870	0.0220	5.50e–5	0.310	0.085	0.0230	0.0450	0.420	1.00	1.00	1.00	
sd(a)/a:	0.10	0.29825	0.46630	0.83285	0.150	0.3011	0.46089	0.37362	0.10092	0		0	
			<i>P(T)</i>	<i>sd(P)</i>	<i>a</i>	<i>sd(a)</i>	<i>b</i>	<i>c</i>	<i>ln K</i>	<i>sd(ln K)</i>			
Independent set of reactions													
gr + q + 2sill = 3an			4.0	1.21	27.05	0.60	0.11540	5.331	7.206	0.886			
2py + 5q + 4sill = 3crd			6.3	0.70	52.59	1.07	0.06314	10.323	5.840	0.980			
2alm + 5q + 4sill = 3fcrd			4.6	0.62	84.16	1.09	0.11292	11.118	4.983	0.944			
py + east + 3q = crd + phl			6.2	1.73	26.15	3.38	0.02664	3.441	3.855	0.677			
3fcrd + 2py + 2east + 6q = 5crd + 2ann			7.3	2.27	81.41	7.27	0.05081	6.667	10.627	1.824			
Average P–T													
<i>T</i> = 747°C													
			sd = 84										
<i>P</i> = 6.5 kbar													
Average P–T calculated from sample Rio-A1, pl–grt(core)–bt(matrix)–kfs–qtz–sill–H ₂ O assemblages													
End-member:	py	gr	alm	phl	ann	east	an	ab	san	ab	q	H ₂ O	sill
Activity (a):	0.0220	5.50e–5	0.310	0.0470	0.0350	0.0250	0.420	0.690	0.890	0.400	1.00	0.500	1.00
sd(a)/a:	0.46630	0.83285	0.15000	0.36805	0.40751	0.45063	0.10092	0.05029	0.05000	0.10800	0		0
			<i>P(T)</i>	<i>sd(P)</i>	<i>a</i>	<i>sd(a)</i>	<i>b</i>	<i>c</i>	<i>ln K</i>	<i>sd(ln K)</i>			
Incomplete, independent set of reactions													
gr + q + 2sill = 3an	3.5	1.14	27.42	0.60	0.11589	5.339	7.206	0.886					
py + 2gr + 3east + 6q = 3phl + 6an	3.6	1.87	29.45	10.14	0.24933	10.706	20.122	2.531					
7phl + 12an = 5py + 4gr + 3east + 4san + 4H ₂ O	8.2	1.66	310.50	10.54	0.16039	22.167	38.036	5.148					
2ann + 3an + 3q = gr + 2alm + 2san + 2H ₂ O	6.9	1.39	62.06	2.17	0.00314	6.307	3.076	1.245					
Average P–T													
<i>T</i> = 851°C													
			sd = 54										
<i>P</i> = 6.5 kbar													
Average P–T calculated from sample Rio-A3, pl–grt(rim)–bt–crd–qtz–sill–H ₂ O assemblages													
End-member:	py	gr	alm	an	phl	ann	east	crd	fcrd	q	H ₂ O	sill	
Activity (a):	0.0160	4.10e–5	0.340	0.410	0.0610	0.0270	0.0370	0.560	0.0800	1.00	1.00	1.00	
sd(a)/a:	0.50357	0.83900	0.15000	0.15000	0.34022	0.44100	0.39138	0.15000	0.30859	0		0	
			<i>P(T)</i>	<i>sd(P)</i>	<i>a</i>	<i>sd(a)</i>	<i>b</i>	<i>c</i>	<i>ln K</i>	<i>sd(ln K)</i>			
Independent set of reactions													
gr + q + 2sill = 3an	3.7	1.30	27.05	0.60	0.11540	5.331	7.427	0.952					
2py + 5q + 4sill = 3crd	5.8	0.78	52.59	1.07	0.06314	10.323	6.531	1.103					
2alm + 5q + 4sill = 3fcrd	4.8	0.64	84.16	1.09	0.11292	11.118	5.420	0.973					
py + east + 3q = phl + crd	5.8	1.84	26.15	3.38	0.02664	3.441	4.055	0.738					
alm + east + 3q = ann + crd	4.0	1.54	27.67	3.51	0.05030	3.731	0.184	0.627					

	$P(T)$	$sd(P)$	a	$sd(a)$	b	c	$\ln K$	$sd(\ln K)$				
<i>Average P–T</i>												
$T = 697^\circ\text{C}$	$sd = 82$											
$P = 5.8\text{ kbar}$	$sd = 0.9$	$cor = 0.841$	$sigfit = 0.59$									
<i>Average P–T calculated from sample Rio-K1, pl–grt(rim)–bt–crd–qtz–sill–H₂O assemblages</i>												
End-member:	py	gr	alm	an	phl	ann	east	crd	fcrd	q	H ₂ O	sill
Activity (a):	0.0260	5.20e–5	0.280	0.450	0.160	0.00950	0.0780	0.590	0.0710	1.00	1.00	1.00
$sd(a)/a$:	0.44574	0.83407	0.15357	0.15000	0.21600	1.05263	0.31166	0.15000	0.32285	0		0
	$P(T)$	$sd(P)$	a	$sd(a)$	b	c	$\ln K$	$sd(\ln K)$				
<i>Independent set of reactions</i>												
$gr + q + 2sill = 3an$	3.7	1.30	27.05	0.60	0.11540	5.331	7.469	0.948				
$2py + 5q + 4sill = 3crd$	6.4	0.71	–52.59	1.07	0.06314	10.323	5.716	0.999				
$2alm + 5q + 4sill = 3fcrd$	4.8	0.67	84.16	1.09	0.11292	11.118	5.389	1.016				
$py + east + 3q = phl + crd$	6.3	1.61	–26.15	3.38	0.02664	3.441	3.840	0.604				
$alm + east + 3q = ann + crd$	7.0	2.37	27.67	3.51	0.05030	3.731	1.360	1.119				
<i>Average P–T</i>												
$T = 723^\circ\text{C}$	$sd = 84$											
$P = 6.5\text{ kbar}$	$sd = 0.9$	$cor = 0.814$	$sigfit = 0.97$									

infer a P – T vector (Fig. 8d). For garnet and cordierite the contours are steep and have negative slopes. They are generally oriented parallel to each other, but deviations from parallelism occur towards lower temperatures. Quartz modes are almost isothermal in the two trivariant stability fields of interest (Fig. 8c). They show increasing modal abundance towards lower temperatures. Reaction (3) consumes garnet and forms cordierite(II) and quartz whereas reactions (4) and (5) involve the breakdown of garnet and K-feldspar to biotite(II), plagioclase and quartz. By combining all information concerning growth and consumption of the phases participating in the reactions, a P – T vector during M_3 that runs roughly parallel to divariant field 2 (indicated in Fig. 8d) towards lower P – T conditions can be inferred to follow peak metamorphism and partial melting.

The clockwise P – T path inferred above can be related to two deformation events. M_1 is interpreted to be contemporaneous with the fabric-forming D_1 event at $P = 6.5\text{ kbar}$ and $T = 750^\circ\text{C}$. The episode of partial melting that formed the M_2 metamorphic peak assemblage occurred also during D_2 . During M_2 , peak temperatures did not exceed 800°C , as the biotite-out line in the calculated pseudosection is not crossed at $P = 6.5$ – 7 kbar . Therefore peak metamorphic conditions for M_2/D_2 deduced from the calculated pseudosection are $T = 750$ – 800°C and $P < 7\text{ kbar}$. In contrast to M_1/D_1 and M_2/D_2 , retrogression that forms the last recognizable

mineral assemblage M_3 occurred during static conditions, thus preventing the rocks from complete re-equilibration under lower-grade conditions, and therefore preserves the observed reaction textures (e.g. garnet breakdown). Retrogression (M_3) is assigned to a period of static decompression and cooling closely following the metamorphic peak.

DISCUSSION

Indications for partial melt loss

For the samples investigated from the Coastal Domain of the Ribeira belt, we have argued that garnet formed by incongruent melting at peak metamorphic conditions. The degree of garnet preservation depends on its proximity to remnants of leucosome (coarse-grained Kfs + Pl + Qtz assemblages). Where garnet is enclosed by leucosome it is strongly resorbed by cordierite–quartz symplectites, whereas it is better preserved where in contact with mesosome. This resorption or preservation of garnet is very localized and differences occur within thin sections. Similar observations have recently been made and discussed in detail by White *et al.* (2001), White & Powell (2002) and Johnson *et al.* (2003), who ascribed preservation of garnet formed during incongruent melting to melt loss. Such melt loss will change the effective bulk composition, thus changing the stable mineral assemblages (Stüwe, 1997), and stabilize garnet to a wider

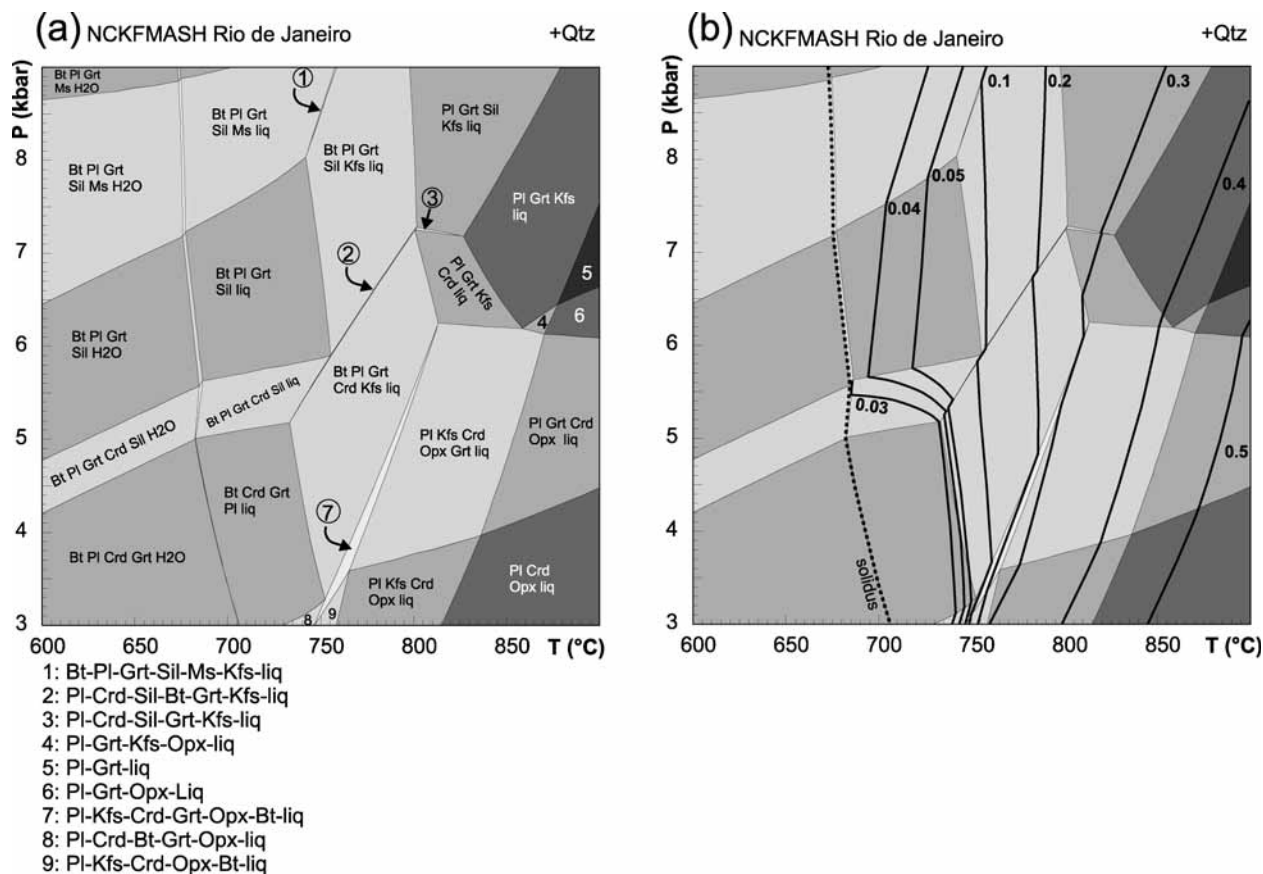


Fig. 7. (a) P - T pseudosection constructed in the model system NCKFMASH ($\text{Na}_2\text{O}-\text{CaO}-\text{K}_2\text{O}-\text{FeO}-\text{MnO}-\text{Al}_2\text{O}_3-\text{SiO}_2-\text{H}_2\text{O}$), using THERMOCALC 3.21 and the internally consistent thermodynamic dataset of Holland & Powell (1998). The bulk composition used was determined by XRF analysis of sample Rio-A3 interpreted to represent the typical composition of the Rio de Janeiro granulites (in mol %: Na_2O 1.27, CaO 1.21, K_2O 2.05, FeO 9.05, MgO 6.11, Al_2O_3 9.55, SiO_2 66.71, H_2O 5). Minerals included in the construction of the grid are garnet (Grt), biotite (Bt), cordierite (Crd), orthopyroxene (Opx), plagioclase (Pl), K-feldspar (Kfs), muscovite (Ms), sillimanite (Sil), melt (liq) with quartz (Qtz) in excess. The fluid phase is assumed to be pure H_2O . Divariant fields (e.g. 7) are light grey; fields with increasingly higher variance are filled with an increasingly darker colour. (b) Summary information for (a), including the solidus and melt mode contours (as molar proportions).

P - T range. If the melt remains *in situ*, garnet will be consumed in a similar way as it was formed by a simple reversion of the initial garnet-forming reaction. This sort of back-reaction appears as retrogression and will tend to produce a mineralogy close to that of the precursor rock (Kriegsmann & Hensen, 1998; Kriegsmann, 2001).

In the case of the investigated granulites, the partial preservation of garnet suggests that the equilibration volume during retrogression was very small. This might be due to two processes or a combination of these: (1) partial melt loss during and/or following peak metamorphism resulting in partial preservation of the peak P - T garnets; (2) deformation during M_2 brings some garnet in contact with melanosome, whereas other nearby garnet still remained in contact with the leucosome.

However, complete back-reaction (*sensu stricto*) should not be expected in the investigated rocks, as the P - T path

of the Rio de Janeiro granulites contains a considerable amount of decompression. Therefore new stability fields are passed and a simple reversion of the prograde reaction is not possible. Hence two processes are important for the preservation of peak metamorphic conditions: (1) partial melt loss and deformation (change of effective bulk composition); (2) decompression (different set of reactions passed). Even though we infer melt loss (partial preservation of garnet) it is difficult to constrain the actual volume lost during partial melting and deformation. Thus it is difficult to discuss the possible pre-melting mineralogy of the investigated rocks. However, parts of the rock that are interpreted as mesosome carry biotite, plagioclase, K-feldspar, quartz and remnants of sillimanite. These minerals may well represent part of the pre-melting assemblage; even garnet might have been part of this assemblage.

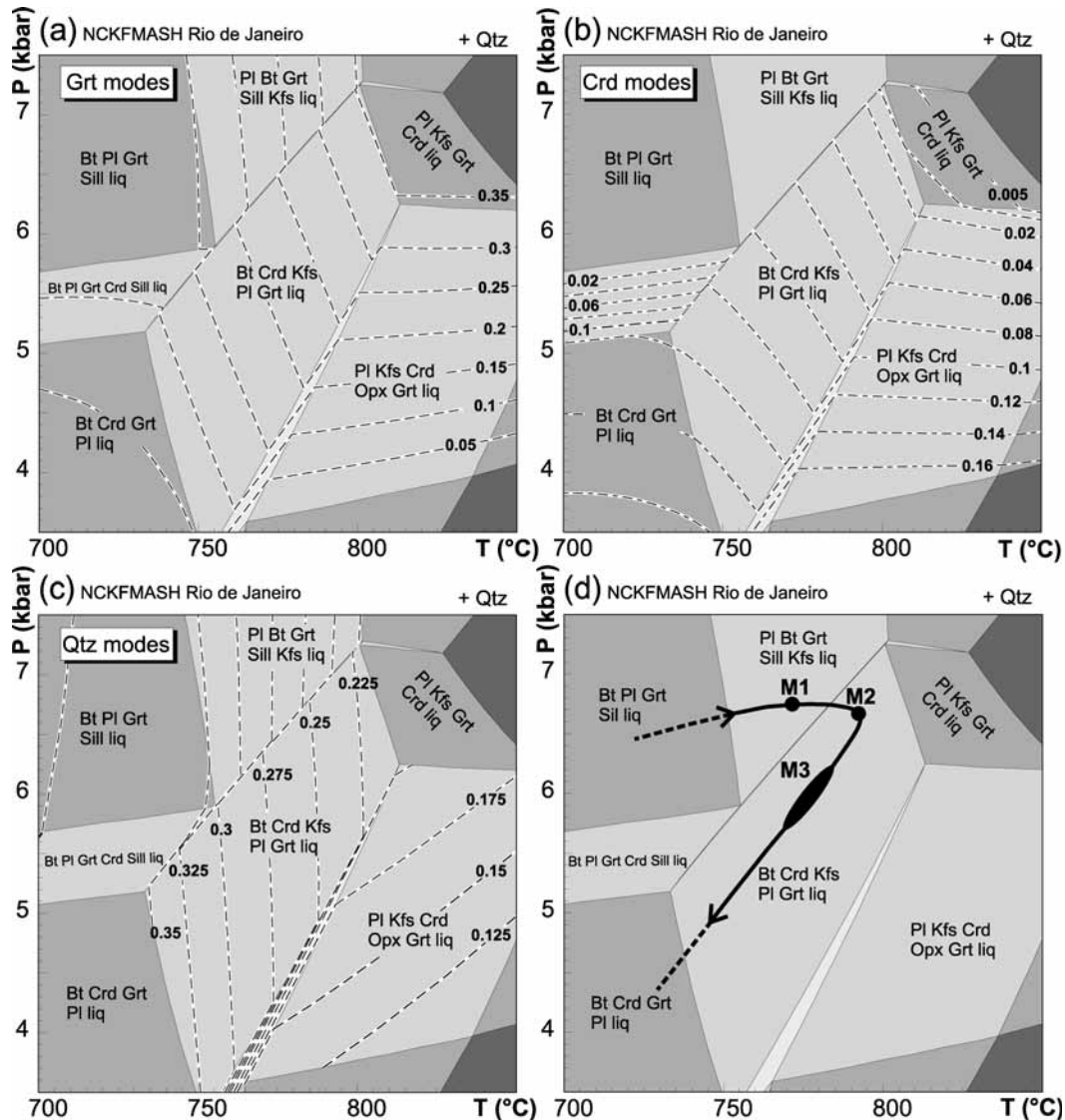


Fig. 8. Sections of the P - T pseudosection shown in Fig. 7 in the P - T range of interest (3.5–7.5 kbar and 700–850°C). (a), (b) and (c) show superimposed isopleths (dashed lines) for garnet, cordierite and quartz, respectively. (d) The path illustrated shows the proposed P - T evolution that satisfies the observed mineral overprinting relationships.

The Rio de Janeiro granulites in the framework of the Ribeira belt

The age of metamorphism, migmatization and magmatism in the Ribeira belt has been constrained to an interval between 591 and 490 Ma of the Brasiliano–Pan-African orogeny (Machado *et al.*, 1996; Brueckner *et al.*, 2000). During this period, three distinct tectonic, metamorphic and magmatic events can be distinguished. A first magmatic and metamorphic phase occurred between 591 and 565 Ma, a second between 555 and 525 Ma and a third event between 503 and 492 Ma. Whereas the first events are phases of accretion and collision between the Congo craton and São Francisco

craton contemporaneous with deformation and syn-collisional intrusion of granitoid plutons, the youngest event is characterized by post-tectonic intrusion of granitoid plutons, stocks and sills (Heilbron & Machado, 2003).

These events span the time frame in which the investigated rocks evolved. The rocks investigated here are petrographically similar to kinzigites dated by Brueckner *et al.* (2000) to 538 Ma that crop out in a similar along-strike position within the Coastal Domain of the Ribeira belt. This may suggest that they formed at a similar time. However, recent attempts to date syn-collisional granulites cropping out in Rio de Janeiro (Silva, 2001; Heilbron & Machado, 2003) yield ages of 560 ± 7 Ma

and 576 ± 1 Ma, respectively. Given the close proximity of these granitoid intrusions to the samples investigated it is reasonable to assume that the studied migmatitic granulites from Rio de Janeiro were formed during collision of the Congo and São Francisco cratons during the Brasiliano orogeny and the syn-collisional intrusion of calc-alkaline plutons into overlying crustal rocks. We conclude that melting and production of the granulites, migmatites and restites found in the Rio de Janeiro realm can be placed in the framework of this major collision and intrusion of various syn-collisional granitoid plutons. We therefore suggest that migmatization in the Rio de Janeiro granulites is related to the first pulse of syn-collisional (arc-related) magmatism and subsequent metamorphism during closure of the Adamastor Ocean.

Heating and cooling mechanisms

The unusually high peak T/P ratios derived above ($>100^\circ\text{C}/\text{kbar}$) are difficult to explain with metamorphism along a 'normal' conductive geotherm: any realistic geotherm through the metamorphic peak conditions would imply lithospheric thicknesses similar to crustal thicknesses and therefore a very unusual tectonic setting (i.e. the 1200°C isotherm is reached at about 50 km depth). Alternatively, a conductive geotherm must have a strong curvature and become near-isothermal just below the Ribeira belt, as has been suggested by Sandiford & Hand (1998) for terrains with high radiogenic heat production (see also McLaren *et al.*, 1999). Unusually highly radiogenic rocks have not been reported from the Ribeira belt, so this model can be excluded as a likely heating source. We, therefore, suggest that the coeval nature of metamorphism and magmatism points to advective heating of the Ribeira metamorphic rocks.

In view of this interpretation, the clockwise $P-T$ path derived for the Rio de Janeiro granulites needs to be explained. Typically, clockwise $P-T$ paths have been interpreted as evidence for conductive thermal regimes because it is thought that cooling from advective heat sources is too rapid to be accompanied by significant depth change and pressure change. For example, if the entire contact metamorphic process occurred over a time scale of the order of 1 Myr and there is negligible burial or exhumation during this time, then the $P-T$ path will be characterized by isobaric cooling. Therefore it needs to be shown that the exhumation rates of the Ribeira belt are comparable with the cooling rates.

To estimate the cooling rates we have designed a very crude thermal model (Fig. 9). This consists of a simple assembly of a series of error function type solutions for step-shaped temperature distributions crudely mapped to represent the two-dimensional surface distribution of intrusions as shown in Fig. 2 [e.g. following the approach

of Jaeger (1964) and Stüwe (2002)]. Figure 9 shows three time steps of this simple model evolution. Figure 9a shows the initial situation at the time of intrusion. It should be noted that the intrusion temperature was assumed to be 1200°C . This was done to mimic the influence of about $400\,000\text{J}/\text{kg}$ of latent heat of fusion in addition to an intrusion temperature of about 800°C . Figure 9b and c shows two time steps in the subsequent evolution. Figure 9d shows temperature–time paths of the three locations sampled for this study. The modelled cooling paths for all three locations have an overall cooling time scale of about half a million years and all three cooling curves are concave towards the time axis and reach metamorphic temperature peaks around 800°C . In view of the simplicity of the model, we suggest that it is meaningless to place any more significance on the shape variations between individual curves. Nevertheless, the rough time scale of cooling places constraints on the rates of pressure change.

The post-peak $P-T$ evolution of the Ribeira belt between M_2 and M_3 is characterized by a ratio of cooling to decompression of $40^\circ\text{C}/\text{kbar}$ (Fig. 8). This corresponds roughly to cooling of 40°C per 3.5 km of depth change. Comparing this with the results of Fig. 9, we can see that roughly 40°C of cooling occurred every 0.1 Myr. The ratio of the estimated cooling rate ($^\circ\text{C}/\text{Myr}$) and the slope of the $P-T$ path ($^\circ\text{C}/\text{kbar}$) is an estimate of the rate of pressure change during the cooling evolution. For the Ribeira belt the numbers above suggest a rate of depth change of around 35 km/Myr. Clearly, this rate is too large to be interpreted in terms of realistic exhumation rates. Although we do not want to suggest a specific mechanism that could be responsible for this apparent contradiction, we give below two possible alternatives.

(1) It is possible that the extreme rates of decompression during cooling are unrelated to depth change, but instead are related to changes in the stress field, generally known under the term 'tectonic overpressure'. The concept of tectonic overpressure lost its significance when experimental rock mechanicians demonstrated that rocks cannot support shear stresses larger than 1 or 2 kbar (Molnar & Lyon-Caen, 1989; Stöckert *et al.*, 1997; Stöckert, 2002). However, as many metamorphic $P-T$ paths are based on <1 kbar of relative pressure change, it is conceivable that $P-T$ paths document stress but not depth changes (Mancktelow, 1993; Stüwe & Sandiford, 1994).

(2) It is possible that the model shown in Fig. 9 grossly underestimates the cooling rates. The overall duration of cooling of a terrain can be estimated from the square of the length scale of the heat source (Jaeger, 1964; Stüwe, 2002). A length scale of 10 km (describing a 10 km thick slab of granitic intrusion below the Ribeira belt) corresponds to a thermal time constant of several million years. Such a duration of cooling is about one order of magnitude larger than that estimated in Fig. 9d, and would

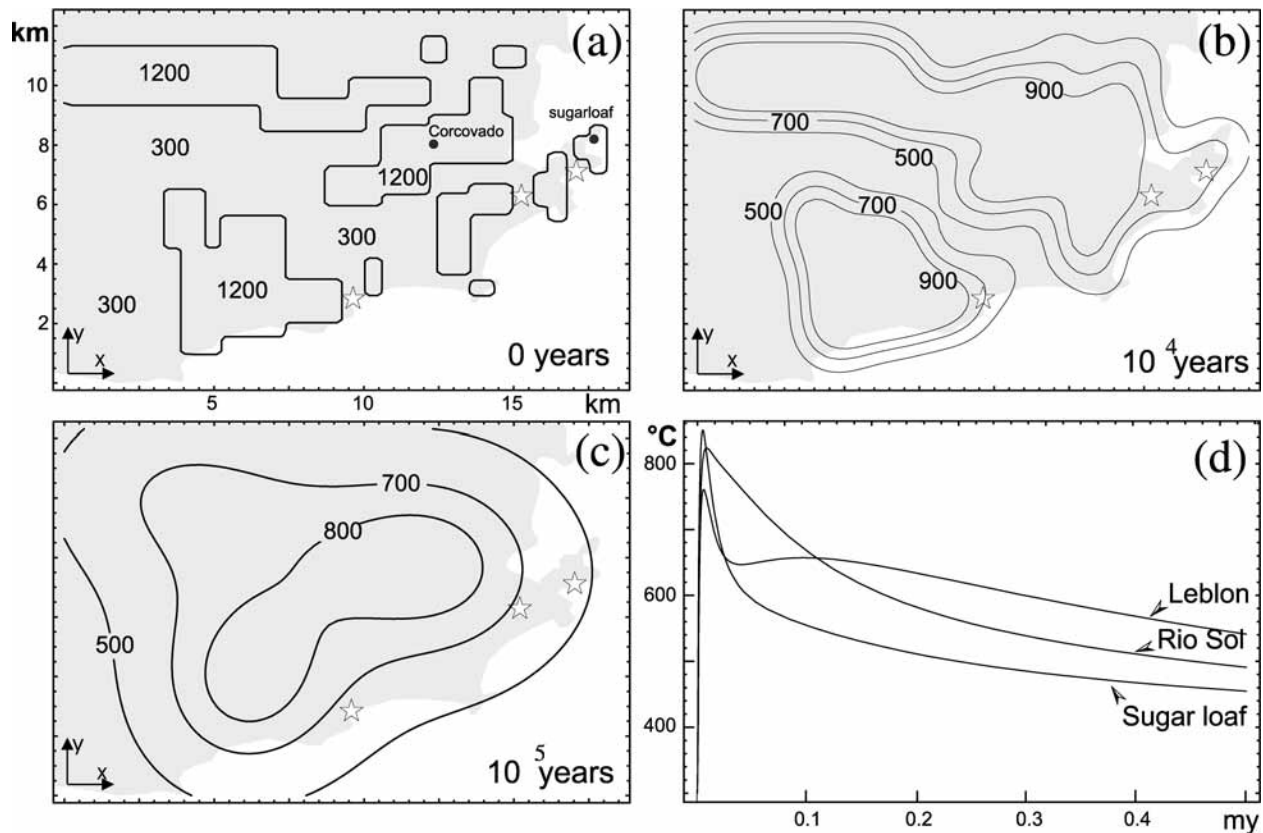


Fig. 9. Model of the thermal evolution of the Rio de Janeiro granulites. (a)–(c) Plan view maps based on Fig. 1 at three time steps after intrusion of the syn-collisional I-type granitoids mapped in detail in Fig. 2b. The land area together with Sugarloaf and Corcovado is shown as a grey background for geographical reference. Sampling locations are marked by open stars. (d) Temperature–time plot for the three sampling locations [open stars in (a)–(c)] and in Fig. 2b. (a) Thermal situation at the time of intrusion; (b) 10 kyr after intrusion; (c) 100 kyr after intrusion. The three temperature–time curves differ in metamorphic peak temperature and shape of the cooling curve largely as a function of distance from the contact of one of the model intrusions. However, it should be noted that all three cooling curves have in common that they reach a metamorphic peak temperature around 800°C and that they converge to a common cooling curve after about 0.5 Myr. Calculation was performed by an appropriate summation of two-dimensional error function type solutions of the diffusion equation [e.g. Jaeger, 1964; Stüwe, 2002, equation (3.93)]. Assumed host rock temperature is 300°C. Assumed intrusion temperature is 700°C. The effect of the latent heat of fusion (about 320 000 J/kg) was described by raising the initial intrusion temperature by 320°C (implicitly assuming a heat capacity of 1000 J/kg K) so that the effective intrusion temperature was assumed to be 1020°.

predict an exhumation rate of only few kilometres per million years. Such an exhumation rate is more realistic and a thickness of 10 km for the intrusions may describe the thermal effects better than the model of Fig. 9.

CONCLUSIONS

(1) Kinzigites from the Ribeira belt in the Rio de Janeiro area preserve a partial record of three mineral assemblages. An M_1 assemblage formed in the sillimanite + biotite stability field during D_1 and is recorded in mesosomes and inclusions in garnet. An M_2 assemblage formed after partial melting during equilibration in the NCKFMASH trivariant field $Bt + Crd + Grt + Pl + Kfs + Qtz + liq$. This assemblage reflects the metamorphic peak and formed during D_2 . An M_3 assemblage formed as a result of static post-peak partial re-equilibration during

decompression. From the three assemblages, a clockwise P – T path may be inferred.

(2) Peak metamorphic conditions involved $T = 750$ – 800 °C and $P < 7$ kbar. These conditions imply a mean geothermal gradient around 40°C/km.

(3) On the basis of the high temperature/depth ratios and contemporaneous *c.* 540 Ma granitoids, we infer that the low- P /high- T metamorphic conditions developed in response to advective heating by these granitoids.

(4) A P – T path involving both decompression and cooling (as derived here) can be reconciled with cooling following ‘contact metamorphism’ only if one of the following processes is considered: (a) it must be shown that the ratio of cooling rate (in°C/Myr) to the slope of the retrograde P – T path (in°C/kbar) has a value that is comparable with realistic exhumation rates recorded from orogenic belts; (b) if this ratio is much too large, it

should be considered whether non-lithostatic stress changes could have an influence on the recorded pressures.

ACKNOWLEDGEMENTS

We thank M. Riesco for his introduction to THERMO-CALC and numerous fruitful discussions concerning pseudosections and their interpretation, and K. Ettinger and J. Neubauer for their help with the SEM analyses. We are grateful to Steve Boger, Alan Whittington and Tim Johnson for their constructive and helpful reviews, which helped to improve the manuscript. This study was carried out within FWF project P-15474-GEO. The revision of this manuscript was finalized while the first author was employed by the DFG-funded Graduiertenkolleg 'Stoffbestand und Entwicklung von Kruste und Mantel' at the University of Mainz. G. Clarke is thanked for his thorough editorial job on the final stages of the manuscript.

REFERENCES

- Alkmim, F. F., Marshak, S. & Fonseca, M. A. (2001). Assembling West Gondwana in the Neoproterozoic: clues from the São Francisco craton region, Brazil. *Geology* **29**, 319–322.
- Bhattacharya, A., Mohanty, L., Maji, A., Sen, S. K. & Raith, M. (1992). Non-ideal mixing in the phlogopite–annite binary, constraints from experimental Mg–Fe partitioning and a reformulation of the biotite–garnet thermometer. *Contributions to Mineralogy and Petrology* **111**, 87–93.
- Brown, M. & Raith, M. (1996). First evidence of ultrahigh-temperature decompression from the granulite province of southern India. *Journal of the Geological Society, London* **153**, 819–822.
- Bruceckner, H. K., Cunningham, D., Alkmim, F. F. & Marshak, S. (2000). Tectonic implications of Precambrian Sm–Nd dates from the southern São Francisco craton and adjacent Araçuaí and Ribeira belts, Brazil. *Precambrian Research* **99**, 255–269.
- Campos Neto, M. C. (2000). Orogenic systems from southwestern Gondwana. In: Cordani, U. G., Milani, E. J., Thomaz Filho, A. & Campos, D. A. (eds) *Tectonic Evolution of South America, 31st International Geological Congress, Rio de Janeiro*, pp. 335–365.
- Carson, C. J., Powell, R., Wilson, C. J. L. & Dirks, P. H. G. M. (1997). Partial melting during tectonic exhumation of a granulite terrane; an example from the Larsemann Hills, East Antarctica. *Journal of Metamorphic Geology* **15**, 105–126.
- Cunningham, D., Alkmim, F. F. & Marshak, S. (1998). A structural transect across the coastal mobile belt in the Brazilian Highlands (latitude 20°S): the roots of a Precambrian transpressional orogen. *Precambrian Research* **92**, 251–275.
- Ellis, D. J. & Green, E. H. (1979). An experimental study of the effect of Ca upon garnet–clinopyroxene Fe–Mg exchange equilibria. *Contributions to Mineralogy and Petrology* **71**, 13–22.
- Ferry, J. M. & Spear, F. S. (1978). Experimental calibration of the partitioning of Fe and Mg between biotite and garnet. *Contributions to Mineralogy and Petrology* **66**, 113–117.
- Fischer, L. H. (1861). Über den Kinzigit. *Neues Jahrbuch für Mineralogie* **1861**, 641–654.
- Ghent, E. D., Black, P. M., Brothers, R. N. & Stout, M. Z. (1987). Eclogites and associated albite–epidote–garnet paragneisses between Yambe and Cape Collett, New Caledonia. *Journal of Petrology* **28**, 627–643.
- Greenfield, J. E., Clarke, G. L. & White, R. W. (1998). A sequence of partial melting reactions at Mt. Stafford, central Australia. *Journal of Metamorphic Geology* **16**, 363–378.
- Guidotti, C. V. (2000). The classic high-*T*–low-*P* metamorphism of west-central Maine; is it post-tectonic or syntectonic? Evidence from porphyroblast–matrix relations; discussion. *Canadian Mineralogist* **38**, 995–1006.
- Hanson, R. B. & Barton, M. D. (1989). Thermal development of low-pressure metamorphic belts: results of two-dimensional numerical modelling. *Journal of Geophysical Research* **94**, 10363–10377.
- Harley, S. L. (1989). The origins of granulites; a metamorphic perspective. *Geological Magazine* **126**, 215–247.
- Heilbron, M. (1995). O segmento central da Faixa Ribeira: síntese geológica e ensaio evolução geotectônica. Tese de Livre Docência, Universidade do Estado do Rio de Janeiro, 140 pp.
- Heilbron, M. & Machado, N. (2003). Timing and terrane accretion in the Neoproterozoic–Eopaleozoic Ribeira orogen (SE Brazil). *Precambrian Research* **125**, 87–112.
- Heilbron, M., Pires, F. R. M., Valeriano, C. & Bessa, M. (1993). Litoestratigrafia, evolução tectono-metamórfica magmatismo precambriano do setor sudeste do município do Rio de Janeiro. In: *Atas III Simpósio de Geologia do Sudeste, Rio de Janeiro, SBG*, pp. 174–179.
- Heilbron, M., Mohriak, W., Valeriano, C. M., Milani, E., Almeida, J. C. H. & Tupinambá, M. (2000). From collision to extension: the roots of the southeastern margin of Brazil. In: Mohriak, W. U. & Talwani, M. (eds) *Atlantic Rifts and Continental Margins. Geophysical Monograph, American Geophysical Union* **115**, 1–32.
- Helmbold, R., Valença, J. G. & Leonardos, O. H., Jr (1964). O mapa geológico do Estado da Guanabara, Rio de Janeiro. DNPM/DGM, scale 1:50 000.
- Hensen, B. J. (1971). Theoretical phase relationships involving cordierite and garnet in the system MgO–FeO–Al₂O₃–SiO₂. *Contributions to Mineralogy and Petrology* **33**, 191–214.
- Hodges, K. V. & Spear, F. S. (1982). Geothermometry, geobarometry and the Al₂SiO₅ triple point at Mt. Moosilauke, New Hampshire. *American Mineralogist* **67**, 1118–1134.
- Holland, T. J. B. & Powell, R. (1998). An internally consistent thermodynamic dataset for phases of petrological interest. *Journal of Metamorphic Geology* **16**, 309–344.
- Jaeger, E. (1964). Thermal effects of intrusions. *Reviews of Geophysics* **2**, 443–466.
- Johnson, T. E., Gibson, R. L., Brown, M., Buick, I. S. & Cartwright, I. (2003). Partial melting of metapelitic rocks beneath the Bushveld Complex, South Africa. *Journal of Petrology* **44**, 789–813.
- Kretz, R. (1983). Symbols for rock-forming minerals. *American Mineralogist* **68**, 277–279.
- Kriegsmann, L. M. (2001). Partial melting, partial melt extraction and partial back reaction in anatexitic migmatites. *Lithos* **56**, 75–96.
- Kriegsmann, L. M. & Hensen, B. J. (1998). Back reaction between restite and melt: implications for geothermobarometry and pressure–temperature paths. *Geology* **26**, 1111–1114.
- Krogh, E. J. (1988). The garnet–clinopyroxene Fe–Mg geothermometer, a re-interpretation of existing experimental data. *Contributions to Mineralogy and Petrology* **99**, 44–48.
- Krogh-Ravna, E. J. (2000). The garnet–clinopyroxene Fe–Mg geothermometer, an updated calibration. *Journal of Metamorphic Geology* **18**, 211–219.
- Lux, D. R., De Yoreo, J. J., Guidotti, C. V. & Decker, E. R. (1986). Role of plutonism in low-pressure belt formation. *Nature* **323**, 796–797.

- Machado, N. (1997). Litogeoquímica e tectônica dos granitóides Neoproterozóicos do Cinturão, Paraíba do Sul no Estado do Rio de Janeiro. Tese de Livre Docência, Universidade do São Paulo, 215 pp.
- Machado, N., Valladares, C. S., Heilbron, M. & Valeriano, C. M. (1996). U/Pb geochronology of the Central Ribeira Belt. *Precambrian Research* **79**, 347–361.
- Mancktelow, N. (1993). Tectonic overpressure in competent mafic layers and the development of isolated eclogites. *Journal of Metamorphic Geology* **11**, 801–812.
- McLaren, S., Sandiford, M. & Hand, M. (1999). High radiogenic heat-producing granites and metamorphism; an example from the western Mount Isa Inlier, Australia. *Geology* **27**, 679–682.
- Molnar, P. & Lyon-Caen, H. (1989). Some simple physical aspects of the support, structure, and evolution of mountain belts. *Geological Society of America, Special Papers* **218**, 179–207.
- Moore, M. A. & England, P. C. (2001). On the inference of denudation rates from cooling ages of minerals. *Earth and Planetary Science Letters* **185**, 265–284.
- Pedrosa-Soares, A. C., Noe, C. M., Wiedemann, C. M. & Pinto, C. P. (2001). The Araçuaí–West-Congo Orogen in Brazil: an overview of a confined orogen formed during Gondwanaland assembly. *Precambrian Research* **110**, 307–323.
- Perchuk, L. L. & Lavrent'eva, N. (1983). Experimental investigation of exchange equilibrium in the system cordierite–garnet–biotite. In: Saxena, S. K. (ed.) *Kinetics and Equilibrium in Mineral Reactions*. Berlin: Springer, pp. 199–240.
- Powell, R. (1985). Regression diagnostics and robust regression in geothermometer/geobarometer calibration: the garnet–clinopyroxene geothermometer revisited. *Journal of Metamorphic Geology* **3**, 231–243.
- Powell, R. & Holland, T. J. B. (1988). An internally consistent thermodynamic dataset with uncertainties and correlations: 3. Application, methods, worked examples and a computer program. *Journal of Metamorphic Geology* **6**, 173–204.
- Powell, R., Holland, T. J. B. & Worley, B. (1998). Calculating phase diagrams involving solid solutions via non-linear equations, with examples using THERMOCALC. *Journal of Metamorphic Geology* **16**, 577–588.
- Sandiford, M. & Hand, M. (1998). Australian Proterozoic high-temperature, low-pressure metamorphism in the conductive limit. In: Treloar, P. J. & O'Brien, P. J. (eds) *What Drives Metamorphism and Metamorphic Relations?* Geological Society, London, *Special Publications* **138**, 109–120.
- Schmitt, R. S., Trouw, R. A. J. & Van Schmus, W. R. (1999). The characterization of a Cambrian (~520 Ma) tectonometamorphic event in the coastal domain of the Ribeira Belt (SE Brazil)—using U/Pb in syntectonic veins. *Special Volume of Expanded Abstracts—II South American Symposium on Isotope Geology*. Córdoba, Argentina: Villa Carlos Paz, pp. 363–366.
- Silva, L. C. (2001). Geologia do Estado do Rio de Janeiro: texto explicativo do mapa geológico do Estado do Rio de Janeiro? Organizado por Luiz Carlos da Silva e Hélio Canejo da Silva Cunha. Brasília: CPRM (CD-ROM).
- Solar, G. S. & Brown, M. (2000). The classic high-*T*–low-*P* metamorphism of west-central Maine; is it post-tectonic or syntectonic? Evidence from porphyroblast–matrix relations; reply. *Canadian Mineralogist* **38**, 1007–1026.
- Stöckhert, B. (2002). Stress and deformation in subduction zones; insights from the record of exhumed metamorphic rocks. In: de Meer, S., Drury, M. R., de Bresser, J. H. P. & Pennock, G. M. (eds) *Deformation Mechanisms, Rheology and Tectonics; Current Status and Future Perspectives*. Geological Society, London, *Special Publications* **200**, 255–274.
- Stöckhert, B., Massone, H. J. & Nowlan, E. U. (1997). Low differential stress during high-pressure metamorphism: the microstructural record of a metapelite from the Eclogite Zone, Tauern Window, Eastern Alps. *Lithos* **41**, 103–118.
- Stüwe, K. (1997). Effective bulk composition changes due to cooling: a model predicting complexities in retrograde reaction textures. *Contributions to Mineralogy and Petrology* **129**, 43–52.
- Stüwe, K. (2002). *Geodynamics of the Lithosphere*. Berlin: Springer, 450 pp.
- Stüwe, K. & Powell, R. (1995). Geothermobarometry from modal proportions. Application to a *PT* path of the Koralm complex. *Contributions to Mineralogy and Petrology* **119**, 83–93.
- Stüwe, K. & Powell, R. (1989a). Metamorphic segregations associated with garnet and orthopyroxene porphyroblast growth; two examples from the Larsemann Hills, East Antarctica. *Contributions to Mineralogy and Petrology* **103**, 523–530.
- Stüwe, K. & Powell, R. (1989b). Metamorphic evolution of the Bungler Hills, East Antarctica; evidence for substantial post-metamorphic peak compression with minimal cooling in a Proterozoic orogenic event. *Journal of Metamorphic Geology* **7**, 449–464.
- Stüwe, K. & Sandiford, M. (1994). On the contribution of deviatoric stress to metamorphic *PT* paths: an example appropriate to low *P* high *T* metamorphism. *Journal of Metamorphic Geology* **12**, 445–454.
- Trompette, R. (1997). Neoproterozoic (600 Ma) aggregation of Western Gondwana: a tentative scenario. *Precambrian Research* **82**, 101–112.
- Trouw, R. A. J., Heilbron, M., Ribeiro, A., Paciullo, F. V. P., Valeriano, C. M., Almeida, J. C. H., Tupinambá, M. & Andreis, R. R. (2000). The central segment of the Ribeira Belt. In: Cordani, U. G., Milani, E. J., Thomaz Filho, A. & Campos, D. A. (eds) *Tectonic Evolution of South America, 31st International Geological Congress, Rio de Janeiro*, pp. 287–311.
- Valladares, C. S., Duarte, B. P., Heilbron, M. & Ragatky, D. (2000). The tectono-magmatic evolution of the occidental terrane and Paraíba do Sul Klippe within the Neoproterozoic Ribeira orogenic belt, southeastern Brazil. *Revista Brasileira de Geociências* **30**, 1–6.
- Vauchez, A., Tommasi, A. & Egydio-Silva, M. (1994). Self-indentation of a heterogeneous continental lithosphere. *Geology* **22**, 967–970.
- Vernon, R. H. (1982). Isobaric cooling of two regional metamorphic complexes related to igneous intrusions in southeastern Australia. *Geology* **10**, 76–81.
- White, R. W. & Powell, R. (2002). Melt loss and the preservation of granulite-facies mineral assemblages. *Journal of Metamorphic Geology* **20**, 621–632.
- White, R. W., Powell, R. & Holland, T. J. B. (2001). Calculation of partial melting equilibria in the system Na₂O–CaO–K₂O–FeO–MgO–Al₂O₃–SiO₂–H₂O (NCKFMASH). *Journal of Metamorphic Geology* **19**, 139–153.